Doctoral Dissertation **Academic year 2012**

Identification of Structural Parameters Using Symbolic Time Series Analysis and Intelligent Algorithms

Keio University

Graduate School of Science and Technology

School of Science for Open and Environmental Systems

Student ID Number 80947888 Name Li, Rongshuai

Thesis Advisor Professor Name Mita, Akira

Keio University
Graduate School of Science and Technology
March 2013

Abstract

Structural Health Monitoring (SHM), a field inaugurated in aerospace engineering in the late 20th century through mechanical engineering towards civil engineering communities. As the process of implementing a damage detection strategy, SHM has received increasingly attention and interest in the civil engineering with prominent technology development and promising economic attraction. Even as research on SHM chugs along, challenges remain before they can be applied to civil engineering structures.

This dissertation presents a new approach for damage identification of structures using symbolization-based intelligent algorithms.

To implement the concept, a two-phase approach is proposed.

In the first phase, a "Symbolization-based Negative Selection" (SNS) algorithm that combines the advantages of symbolic time series analysis (STSA) and negative selection (NS) is proposed for detecting the abnormal states of a building structure. In SNS, no prior knowledge of the structure's abnormal state is needed. Only the response of the structure in a current normal state is used as input data. In addition, this approach works fine even with one sensor, so it is highly practical and flexible.

In the second phase, after knowing the damage occurrence, we need to determine the damage location and quantity. The method for this stage was named as “Symbolization-based Differential Evolution Strategy” (SDES). Differential evolution

(DE) strategy employed here is intended to minimize the distance between SSHs (state sequence histogram) that are transformed from raw acceleration data of a real structure and candidate models. Accuracy of the method is theoretically studied and explained including the effects of parameters. SDES was numerically compared with Particle Swarm Optimization (PSO) and DE with raw acceleration data. These simulations revealed that SDES provided better estimates of structural parameters when the data was contaminated by noise.

Moreover, in order to prove that the method is indeed applicable to realistic problems, the computing strategy for SHM is experimentally verified. Two different structural models, small model and large steel model, are utilized to verify the proposed approach. Experiments using the small model were conducted at our Laboratory, damage cases were considered for different locations and degrees of damage. Data of the experiments using the steel model (carried out under the US–Japan cooperative structural research project on Smart Structure Systems) was used to further verify the proposed methodology.

Finally, the conclusion is given. The damage identification using symbolic time series analysis and intelligent algorithms is proposed, and it can detect, localize and quantify the damage accurately. The symbolization of data alleviates the effects of harmful noise, employment of the intelligent algorithms make the whole procedure adaptively and efficiently. Comparisons with existing methods show that our proposed methodology is indeed a powerful tool for damage identification of building structures.

Acknowledgements

Many thanks to Professor Akira Mita, my advisor, for his constant encouragement and guidance. Without his consistent illuminating instruction and broad-ranging professional view, this dissertation could not have reached its present form. The positive attitude to face problems and dauntless courage to overcome difficulties, enlightened by his persistent determination and true benevolence, are most valuable treasures in the research work and in my life. Thanks, sensei, more than I can say.

I would like to express my gratitude to Professor Hiromitsu Ohmori, Professor Nozomu Hamada and Associate Professor Masayuki Kohiyama for reviewing this thesis thoroughly and giving me valuable comments.

Many thanks to Professor Songtao Xue at Tongji University, who led me into this field of structural health monitoring, for his great kindness, high responsibility and continual support in the past six years.

Many thanks to the students at Mita Laboratory and friends at Keio University who gave me countless warm help and friendship.

And finally never enough thanks to my beloved family for their loving considerations and great confidence all through these years.

Contents

Figures

Tables

CHAPTER 1
Introduction

1.1 Structural Health Monitoring

Structural health monitoring (SHM) for the prediction of onset damage and deterioration of building structures has increasingly received attention and interest because of the rising numbers of aged infrastructure and high damage costs caused by unpredictable hazards. In July 2007, New York suffered from the explosion of an 83-year-old steam pipe, and Americans were horrified to see a bridge filled with commuter traffic collapse across the Mississippi River. In 2011, a 9.0-magnitude (Mw) undersea megathrust earthquake occurred on 11 March in Tōhoku, Japan. The quake lasted approximately six minutes, and it destroyed many structures in north eastern Japan and caused a crisis at a nuclear power plant.

The process of implementing a damage detection and characterization strategy for engineering structures is referred to as Structural Health Monitoring (SHM) (Mita, 2003). The SHM process involves the observation of a structure over time using periodically sampled measurements from an array of sensors, the extraction of damage-sensitive features from these measurements, and the statistical analysis of

these features to determine the current state of structural health. For long term SHM, the output of this process is periodically updated information regarding the ability of the structure to perform its intended functions in light of the inevitable aging and degradation resulting from operational environments. After extreme events, such as earthquakes or blast loading, SHM is used for rapid condition screening and aims to provide, in near real time, reliable information regarding the integrity of the structure (Cempel, 1980; Auweraer and Peeters, 2003; Farrar and Worden, 2007).

The SHM problem is fundamentally one of a statistical pattern recognition paradigms (Sohn et al., 2004; Hayton and Utete, 2007). The paradigm can be divided into four parts:

1) Operational Evaluation,
2) Data Acquisition, Fusion, and Cleansing,
3) Feature Extraction and Information Condensation,
4) Statistical Model Development for Feature Discrimination.

1.2 Definition of Damage

Damage is defined as changes to the material or geometric properties of a structural system, including changes to the boundary conditions and system connectivity, which adversely affect the system's performance. According to the amount of information provided regarding the damage state, the damage identification can be classified into four levels (Rytter, 1993):

Level 1: Damage Existence. Is there damage in the system?

Level 2: Location. Where is the damage in the system?

Level 3: Extent. How severe is the damage?

Level 4: Prognosis. How much useful life remains?

Answers to these questions in order represent increasing knowledge of the damage state. When applied in an unsupervised learning mode, statistical models are typically used to answer questions regarding the existence and location of damage. When applied in a supervised learning mode and coupled with analytical models, the statistical procedures can be used to better determine the type of damage, the extent of damage and remaining useful life of the structure. The statistical models are also used to minimize false indications of damage (Farrar and Worden, 2007).

False indications of damage fall into two categories:

1) False-positive damage indication (indication of damage when none is present),

2) False-negative damage indication (no indication of damage when damage is present).

Errors of the first type are undesirable, as they will cause unnecessary downtime and consequent loss of revenue as well as loss of confidence in the monitoring system. More importantly, there are clear safety issues if misclassifications of the second type occur. Many pattern recognition algorithms allow one to weigh one type of error above the other; this weighting may be one of the factors decided at the operational evaluation stage (Hayton and Utete, 2007; Sohn, 2007).

1.3 Damage Detection Methods

The main parts of the SHM in civil engineering are damage detection, localization and quantification, which are essential monitoring zones for structures after major events

such as earthquakes (Mita, 2003).

1.3.1 Statistical Discrimination of Features for Damage Detection

In general, structural identification for health monitoring involves the comparison of the changes in structural properties or response, and it can be viewed as a pattern classification problem. In the case of structural identification, damage is usually described as the decrease in structural parameters such as the stiffness of structural members. Effective pattern classification or interpretation of the changes in structural response or dynamic properties due to damage is a critical task. The fundamental idea of the pattern classification approach is to use training data obtained from simulation calculation to determine the classifier referred to as training the classifier and according to the classifier to evaluate the category of the test data. However, a very large database is required to store training data for as many damage cases as one may wish to consider. In general, damage cases of single-damage and multiple-damage with different and/or the same damage extents should be considered.

1.3.2 Modal Properties Based Damage Detection Methods

Modal properties based damage detection methods mainly include damage detection using frequency and modal shape. The forward and the inverse identification by employing frequency analysis, which both assume that natural frequency of a structure shifts when the damage occurs, can be used for damage identification (Hearn and Testa, 1991; Ljung, 1999; Vestroni and Capecchi, 2000; Peeters, Maeck et al. 2001; Kessler, Spearing et al. 2002; Kim, Ryu et al. 2003). Cawley and Adams (1979) give a formulation to detect damage in composite materials from frequency shifts. Friswell, et al. (1994) present the results of an attempt to identify damage based on a

known catalog of likely damage scenarios. The authors presumed that an existing model of the structure is highly accurate. Using this model, they computed frequency shifts of the first several modes for both the undamaged structure and all the postulated damage scenarios. Williams and Messina (1999) formulated a correlation coefficient that compares changes in a structure's resonant frequencies with predictions based on a frequency-sensitivity model derived from a finite element model. For damage identification using modal shape analysis, West (1986) and Wolff and Richardson (1989) suggested the use of the modal assurance criterion (MAC) to detect the existence and the location of structural faults. Yao and Natke (1994) present a model-based approach for damage detection and structural reliability evaluation based on parameter changes of the verified mathematical model. Modal tests of a full-scale bridge before and after rehabilitation was conducted by Salawu and Williams (1995), the conclusion is that the natural frequencies of the bridge did not change much as a result of structural repairs whilst.

1.3.3 Current Methods Involving Statistical Pattern Recognition Using Time Series Domain

Many damage detection algorithms are based on the study of the modal properties of a structure such as modal frequencies, mode shapes, curvature mode shapes and modal flexibilities. However, the use of modal properties involves loss of information, in particular about the precise location of the damage and its magnitude because of the global signification of such tools. Indeed, modal properties are independent of the excitation signal characteristics (like amplitude and frequency) and the location of the excitation. Thus, it may be difficult for global properties to identify local damages apart from severe ones. Moreover, the modal-based methods often rely on the finite element method which is very time-consuming. Time-series-based methods, which are

an important component of vibration-based methods, coupled with statistical pattern recognition, offer several alternatives to these limitations as modal-based methods. Sohn and Farrar (2001) proposed the damage diagnosis method that uses the time-series analysis of vibrating signals. A study by Xue et al. (2009) applied an auxiliary particle filtering (APF) method to track a dynamic system with sudden parameter changes. Guo and Li (2011) introduced a damage detection method based on strain energy, and the evidence theory was presented in order to solve the damage detection problem. Bernal and Hernandez (2006) presented a data-driven methodology for assessing impact of earthquakes on the health of building structural system. Wan and Mita (2009) used acoustic principal component analysis recognition with the Mel scale for pipeline monitoring. Zheng and Mita (2007, 2008) defined the distance between ARMA models as a damage indicator and proposed a two-stage damage diagnosis method. Lynch et al. (2006) explored the use of wireless sensors as building blocks of future structural health monitoring systems. Li and Mita (2011) used an improved clonal selection algorithm (CSA) for damage identification based on raw acceleration data. An approach using the support vector machine (SVM) to detect local damages in a building structure was proposed by Mita and Hagiwara (2003). Xing and Mita (2011) did local damage detection of shear structures by using a substructure approach. These techniques are really interesting because it only requires data from the undamaged structure in the training phase, also known as unsupervised learning. Gul et al. (2009) used features from autoregressive models in conjunction with Mahalanobis distance-based outlier detection algorithms to identify several types of structural changes on different structures. Sohn et al. (2000) analyzed the coefficients of auto-regressive models by using X-bar control charts. Most of the present studies use damage-sensitive features issued from the time-series data in order to detect and localize damages. Some studies were lead by using raw time-series data. Xu et al. (2003) used acceleration, velocity and displacement time histories as inputs

to the emulator neural network. Qian and Mita (2008) used directly acceleration time histories as input of artificial neural network in order to detect damage occurrence. By using raw time-series data without extracting any sensitive features, the studies have shown that damage detection can efficiently be carried out. However, any information about damage localization can be provided.

1.3.4 Current Methods Involving Artificial Immune Systems for Anomaly Detection

To the author's knowledge, this research is novel in terms of applying artificial immune systems for structural damage detection in civil engineering structures. Indeed, most of the studies in this field were conducted on mobile robots, aircrafts, ECG (Electrocardiography) signals or milling operations as it is explained below.

One of the first research applying artificial immune systems to fault or anomaly detection was lead by Dasgupta and Forrest (1995). In this research, tool breakage detection in milling operations was successfully conducted from dynamic variation of the cutting force signals. In this research, the immune algorithm required a lot of time (exponential to the size of the normal data set) and produced fault detectors in a random way. Thus, the abnormal space was inefficiently covered.

Dasgupta et al. (2002) proposed an aircraft fault detection inserted in an intelligent flight control based on a real-valued negative selection algorithm for detection of control surface area loss. This algorithm tried to cover as efficiently as possible the nonself space. However, the localization problem was not tackled. Indeed, aircrafts were tested for engine failure, wing failure or full tail failure. Thus, the knowledge of the damage was enough considering that localization was treated before by the knowledge of the analysed signal. Strackeljan and Leiviska (2008) developed a fault detection method for rolling bearings by using an artificial immune network called

AbNet. The results were promising but any damage localization was studied. The presented methods only used one method from artificial immune systems. There were also other studies which try to combine artificial immune systems with other classification techniques. Dasgupta and Kozma (2002) proposed an anomaly detection process using negative selection and classification technique such as multilayer neural network or an evolutionary algorithm generating fuzzy classifier rules. Bereta and Burczynsky (2006) developed a feature selection and classification process for ECG signals combining two different models of artificial immune systems, clonal selection followed by negative selection. In this research, the knowledge of abnormal or nonself data is compulsory but in civil engineering problems, nonself is usually unavailable.

1.3.5 Symbolic Time Series Analysis

Recently, Ray and coworkers (2004, 2006 and 2007) developed a novel pattern identification technique called “symbolic dynamic filtering” (SDF). The core concept of SDF is built on the identification of statistical patterns from symbol sequences generated by coarse-graining of time series data (Ray, 2004). These statistical patterns represent the behavior of a dynamical system, which may change with the evolution of anomalies. SDF has been shown to yield superior performance in terms of early detection of anomalies and robustness to measurement noise in comparison to other techniques such as Principal Component Analysis (PCA), Neural Networks (NN) and Bayesian techniques (Rao et al., 2009). Recently, in a two-part paper (Gupta et al., 2011; Sarkar et al., 2008), an SDF-based algorithm for detection and isolation of engine subsystem faults (specifically, faults that cause efficiency degradation in engine components) has been reported and an extension of that work to estimate simultaneously occurring multiple component-level faults has been presented in (Sarkar et al., 2009). Furthermore, an optimized feature extraction technique has been developed under the same semantic framework in (Sarkar et al., 2011). However, all

of the above studies were conducted on steady-state cruise flight data that conform with the assumption of quasi-stationary made in SDF. Due to this assumption, SDF may not be able to adequately handle transient data that are usually of limited length.

1.4 Challenge

Even as research on SHM chugs along, challenges remain before they can be applied to civil engineering structures. Most currently available damage detection methods are global in nature, i.e., the dynamic properties (natural frequencies and mode shapes) are obtained for the entire structure from the input–output data using global structural analyses. However, natural frequencies and mode shapes are not sensitive to minor damage and local damage.

Although progress has been made due to employment of intelligent algorithms in SHM, there are two big problems in these existing methods. One is that prior knowledge of a structure's abnormal state is needed. To achieve this, a numerical model of the structure is needed, but as a complex system, a proper model that can describe the dynamics of building structures is very hard to create. Even some dynamical systems may be modeled by a lumped mass system with masses, springs, and dashpots; however, the values of masses, springs, and dashpots for a system are usually not the same as those estimated from the structure design. This makes the whole procedure impracticable. The other is that occurrence of noise in the response of structures always makes it difficult to extract the dynamic features of structures, which will also affect the accuracy and feasibility of the procedure. In such a case, abnormal state detection of building structures should be to evaluate the new state of structure health based on the existing healthy state of structures. A novel indicator which is sensitive to structure parameters but not to environmental factors should be created.

1.5 Organization of Thesis

This thesis is divided into six chapters as below.

Chapter 1 gives a brief introduction of SHM and damage detection.

Chapter 2 presents strategies of data symbolization by using symbolic time series analysis (STSA). Data symbolization alleviates the effects of harmful noise in raw acceleration data. Different types of symbolization strategies and corresponding advantages and disadvantages are compared. The internal mechanisms of noise immunity, effect of parameters and solution range of STSA are explained mathematically.

Chapter 3 proposes a symbolization-based negative selection (SNS) algorithm that combines the advantages of symbolic time series analysis (STSA) and negative selection (NS) for detecting the abnormal states of building structures. In SNS, no prior knowledge of a structure's abnormal state is needed. Only the response of the structure in a current state is used as input data. In addition, this approach works fine even with one sensor, so it is highly practical and flexible. A state sequence histogram (SSH) transformed from raw acceleration data by using STSA can capture the main features of structure dynamics and alleviate the effects of harmful noise. SSHs of the normal and abnormal states of a structure are defined as self and non-self elements, respectively. A new detector generation strategy and matching mechanism is proposed that makes the procedure more effective, along with guidelines for appropriate parameters in SNS. Numerical simulations for different abnormal state cases were conducted to demonstrate the feasibility of the proposed method.

Chapter 4 presents a new method of identifying structural parameters, called “Symbolization-based Differential Evolution Strategy” (SDES), merges the advantages of Symbolic Time Series Analysis (STSA) and Differential Evolution

(DE). Data symbolization in SDES alleviates the effects of harmful noise. SDES was numerically compared with Particle Swarm Optimization (PSO) and DE on raw acceleration data. These simulations revealed that SDES provided better estimates of structural parameters when the data was contaminated by noise. SDES performed much better than PSO and DE on raw acceleration data. The simulations show that SDES is a powerful tool for identifying unknown parameters of structural systems even when the data is contaminated with relatively large amounts of noise.

Chapter 5 presents experimental verifications. A five-story structure was initially healthy with all original columns intact. Two columns of one floor were then replaced by weak columns (of the same material and integrity with healthy columns, but with smaller cross-sectional area) to simulate single-damage case. The double-damage and triple-damage case was simulated by replacing the columns of two or three different floors, respectively. Under the basement of the structure, there were some bearings so that the structure could have a ground motion. Another steel structure on a shake-table was used to verify the proposed method. It was also a five-story frame structure, with a height of 5m and a floor slab of 3m x 2m. The damages were introduced by removing the splices at different location, loosing the bolts and damaging the beams. The experimental results have shown that the proposed approach can successfully monitor structural health only by utilizing measured acceleration information for various damage scenarios under different excitation conditions. The proposed approach was shown promising for application of SHM to buildings.

Chapter 6 summarizes contributions of this thesis, and points out the direction for future works.

CHAPTER 2
Symbolic Time Series Analysis

2.1 Introduction

An important advantage of STSA is its robustness to measurement noise (Rajagopalan and Ray, 2006). It is expected that small changes in time series data do not affect the symbolized data. Therefore, it can be assumed that a certain band of states represents similar dynamic status of the dynamic structural system.

This chapter explains the basic principle behind symbolic time series analysis (STSA). The procedure to symbolize raw acceleration will be explained in detail, different type of symbolization strategies will be described and compared. As detailed information of raw acceleration data may be missed during the process of STSA, the effect of parameters in STSA is verified mathematically, internal mechanisms of noise immunity is explained and a novel procedure to verify the solution range of the procedure is proposed to demonstrate that acceptable results can be obtained by employing STSA to symbolize the raw acceleration data.

2.2 Classical Data versus Symbolic Data

It may be appropriate to say that while the classical data analysis focuses on individuals, symbolic data analysis deals with concepts, a less specific type of information. Through symbolic conversion, the original time series signals are converted into sequences of discrete symbols.

Consider a structural system Σ, raw data of acceleration response $\{\ddot{x}_0, \ddot{x}_1, \dots, \ddot{x}_{T-1}\}$ (T is window length) can be recorded using sensors. The first step is to transform the raw acceleration data into binary symbol series $\{\sigma_0, \sigma_1, \dots, \sigma_{T-1}\}$, σ_i $(i \in [0, T-1])$ equals to '0' or '1' due to partition strategy. After that, we select an integer r $((T-1) > r \geq 1)$ as word length and define the symbolic state at the time t as the vector s_t containing the follow-up r output symbols, namely,

$$s_t = [\sigma_t, \sigma_{t+1}, \dots, \sigma_{t+r-1}],\ t \in [0, T-r+1] \tag{2.1}$$

s_t defines a state series $\{s_0, s_1, \dots, s_{T-r+1}\}$. Binary coded s_t should be transformed into decimal domain, and note that s_t can take $Q = 2^r$ possible values (called states), which can be listed in a finite set $S = \{0,1, \dots, Q-1\}$. We then can derive the statistics of the symbolic state, i.e., compute the vector of the observed state frequencies $D = [d^0, d^1, \dots, d^{Q-1}]$, where d^i (integer $i \in [0, Q-1]$) is the number of occurrences of $S = i$. Also D can be normalized by $\frac{D}{T-r+1}$.

In the example shown in Figure 2.1, sampling points of raw acceleration data series are shown as small circles which have different values, where the x axis stands for time and the y axis acceleration. A line with value 0 (here it is just the x axis) is chosen as partition line. Thus, the whole space is separated into two regions (one is value of acceleration data equal to or bigger than 0, the other is value of acceleration

data smaller than 0). The acceleration data that falls inside the upper region is symbolized as '1'; otherwise, it is '0'. After the symbolization, a binary coded symbol series which only contained '0' and '1' can be obtained. In this example, a word length of 3 is used to create words, which means the first three symbols '1 0 0' is chosen as the first word, the second to fourth symbols '0 0 0' is chosen as the second word, repeating the procedure and 24 words can be created from the symbol series. Every binary coded word needs to be transformed to the decimal domain, take the first word as an example, '1 0 0' can be transformed to 4 ($1 \times 2^2 + 0 \times 2^1 + 0 \times 2^0$), which is called as a state. A state series can be obtained after all the words are transformed from the binary domain to the decimal domain, which is constituted with values 0 to 7.

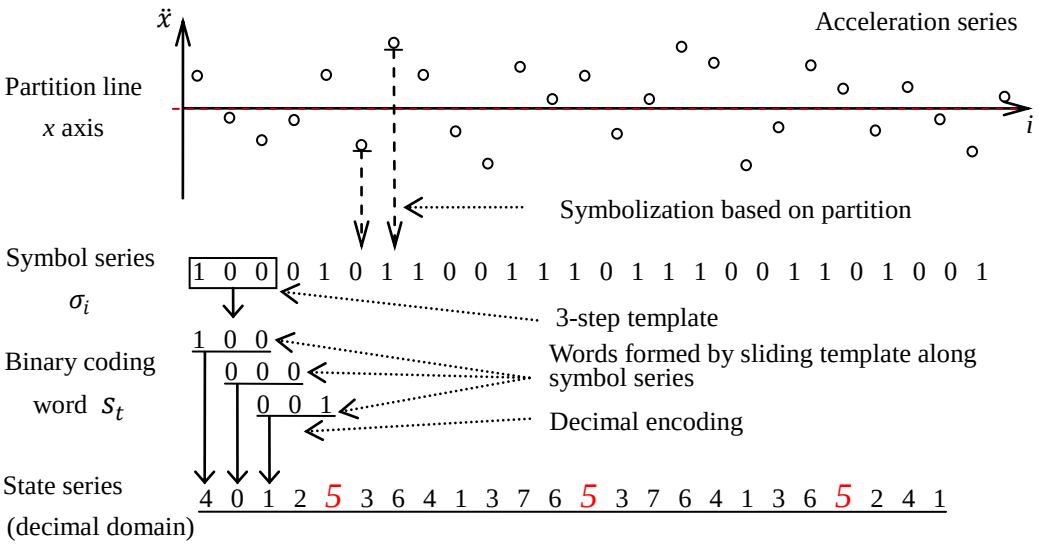

Figure 2.1. Process of symbolizing a time series of accelerations with "Zero" strategy (T = 26 and r = 3)

As shown in Figure 2.1, the occurrence number of a certain state in the state series is different. A bar graph of plotting the occurrence number of every state in the state series is called State Sequence Histogram (SSH). Corresponding SSH of this example

is plotted in Figure 2.2(a). Taking state '5' as an example, corresponding count number is '3', means that state '5' occurred 3 times in the state series (as marked in the state series of Figure 2.1). And also SSH can be normalized, which can be accomplished by dividing occurrence number of each state by the total number of states in the whole state series, which is shown in Figure 2.2(b).

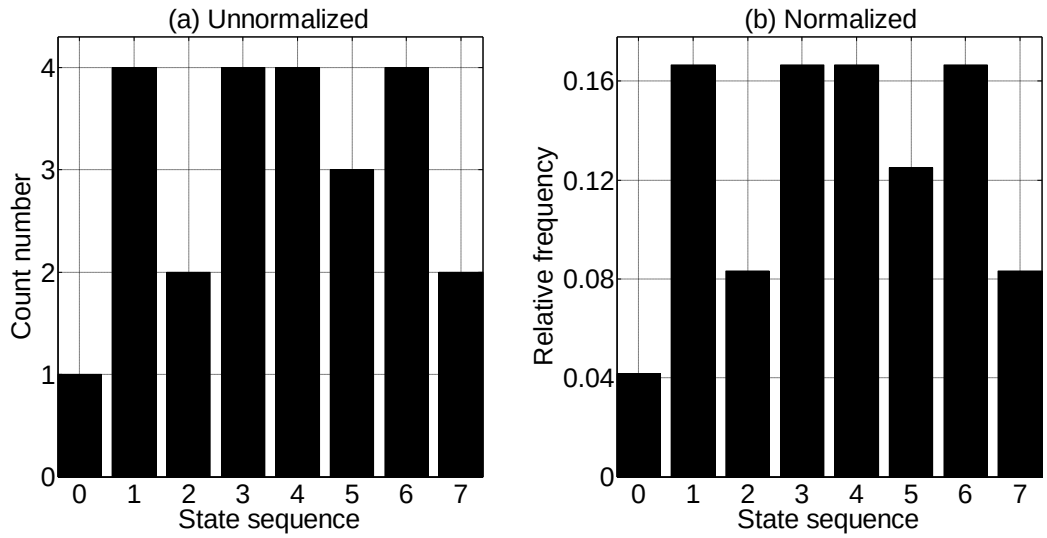

Figure 2.2. Corresponding unnormalized and normalized state sequence histogram (SSH) of the example in Figure 2.1 (T = 26 and r = 3)

2.3 Types of Symbolization Strategy

As there are different strategies for symbolizing a time series data, three of them will be introduced here. For the difference among them is just the step of transforming the raw acceleration data to symbol series, but keeps the other steps like choosing word, transforming binary coded word to decimal domain and the step of calculating the SSH unchanged, only the difference will be declared here.

The first one is called "Zero" strategy, which can be explained just using the example of Figure 2.1. The main specialty of this strategy is using a line with zero value as the

partition line.

The second one is called "Mean" strategy. The difference between "Mean" and the "Zero" strategy is that "Mean" strategy using line of mean value of the raw acceleration data series as partition line instead of a line with zero value in "Zero" strategy.

Obviously, the "Zero" and "Mean" strategies have a disadvantage as they may miss very detailed signals. To represent such details, the third strategy, "1st order difference" strategy should be employed. Note that for this strategy, there is no partition line like that used in "Zero" and "Mean" strategies. The main principle of "1st order difference" is contrasting every single acceleration value with the previous one from the second value of the raw acceleration series, if it is bigger than or equal to the previous one, one '1' symbol will be created, else the symbol will be created as '0'. This strategy extracts details on the composition from the signal, but it is affected by noise much more easily than the "Zero" and "Mean" strategies are. The main procedure of 1st-order difference strategy is shown in Figure 2.3.

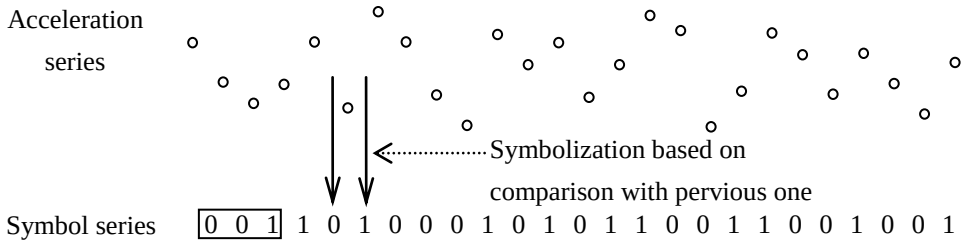

Figure 2.3. Symbolization with 1st-order difference partition strategy (T = 26 and r = 3)

The coding procedure of three partition strategies are summarized and listed in Table 2.1. Where T is the window length, $\ddot{x}_i$ is the acceleration value at step $i \in [0, T-1]$.

Table 2.1. Process of symbolization with different partition strategies

Zero	Mean	1st order difference
for i = 0: T − 1	for i = 0: T − 1	for i = 1: T − 1
if ẍ$_i$ ≥ 0	if ẍ$_i$ ≥ mean(ẍ)	if ẍ$_i$ ≥ ẍ$_{i-1}$
symbol(i) = 1;	symbol(i) = 1;	symbol(i) = 1;
else	else	else
symbol(i) = 0;	symbol(i) = 0;	symbol(i) = 0;
end	end	end
end	end	end

2.4 Effect of Parameters in STSA

In STSA, the main parameters are word length r and window length T, which control the resolution of the whole representation space.

In this research, we introduce an index, the relative state sequence histogram error (RSSHe), to measure the distance between SSH_a and SSH_b. The definition is:

$$SSH_a = \left[d_a^0, d_a^1, \dots, d_a^{Q-1}\right], SSH_b = \left[d_b^0, d_b^1, \dots, d_b^{Q-1}\right], Q = 2^r.$$

$$RSSHe = \sqrt{\frac{\sum_{i=0}^{Q-1}(d_b^i - d_a^i)^2}{\sum_{i=0}^{Q-1}(d_a^i)^2}} \tag{2.2}$$

where d_a^i and d_b^i are the frequency of state i in SSH_a and SSH_b, respectively.

For window length T and word length r, two limiting cases of a SSH are predefined as:

Case 1: All states in a SSH are distributed uniformly, and the frequency of each state is $\frac{1}{2^r}$.

Case 2: Only one state in a SSH has a frequency of 1, and the frequency of the other states is 0.

Suppose there are two different $SSHs$: SSH_a and SSH_b. From Equation (2.2), when SSH_a corresponds to the limiting case 1 and SSH_b to the limiting case 2, the maximum value of $RSSHe$ is:

$$RSSHe_{max} = \sqrt{\frac{\sum_{i=0}^{Q-1}(d_b^i - d_a^i)^2}{\sum_{i=0}^{Q-1}(d_a^i)^2}} = \sqrt{\frac{(1-\frac{1}{2^r})^2 + \left(\frac{1}{2^r}\right)^2 (2^r - 1)}{(\frac{1}{2^r})^2 \cdot 2^r}} = \sqrt{2^r - 1} \qquad (2.3)$$

When SSH_a and SSH_b are the same, the minimum $RSSHe$ is 0. Then,

$$RSSHe \in [RSSHe_{min}, RSSHe_{max}] = [0, \sqrt{2^r - 1}] \qquad (2.4)$$

Since the minimum changeable unit in SSH is $\frac{1}{T-r+1}$, the frequency change of one state in SSH will absolutely be related to the change of frequency of other states. Supposing that there are only two minimum unit differences between SSH_a and SSH_b, then the minimum distinguishable $RSSHe$ is:

$$RSSHe_{dis} = \sqrt{\frac{\sum_{i=0}^{Q-1}(d_b^i - d_a^i)^2}{\sum_{i=0}^{Q-1}(d_a^i)^2}} = \sqrt{\frac{(\frac{1}{T-r+1})^2 + (\frac{1}{T-r+1})^2}{\sum_{i=0}^{Q-1}(d_a^i)^2}} = \frac{\sqrt{\frac{2}{\sum_{i=0}^{Q-1}(d_a^i)^2}}}{T-r+1} \quad (2.5)$$

When SSH_a is the limiting case 1, the maximum distinguishable $RSSHe_{dis}^{max}$ will be:

$$RSSHe_{dis}^{max} = \frac{\sqrt{2^{(r+1)}}}{T-r+1} \quad (2.6)$$

When SSH_a is the limiting case 2, the minimum distinguishable $RSSHe_{dis}^{min}$ will be:

$$RSSHe_{dis}^{min} = \frac{\sqrt{2}}{T-r+1} \quad (2.7)$$

The resolution is:

$$\left[RSSHe_{dis}^{min}, RSSHe_{dis}^{max}\right] = \left[\frac{\sqrt{2}}{T-r+1}, \frac{\sqrt{2^{(r+1)}}}{T-r+1}\right] \quad (2.8)$$

Note that we also need to consider the number of the possible distributions of states in one SSH. If the number of states in SSH is 2^r and the minimum changeable unit is $\frac{1}{T-r+1}$, then the total number of possible distributions N_{SSH} of SSH is equal to one classic combination problem, which is 'put the $T-r+1$ same balls in 2^r different

boxes, and the combinatorial number is:

$$N_{SSH} = \binom{T - r + 2^r}{2^r - 1} \tag{2.9}$$

As we can see, a bigger value for the window length and word length is related to a higher resolution, which is the foundation for obtaining acceptable results in system identification.

2.5 Internal Mechanisms of Noise Immunity

In the research field of system identification, usually we choose the raw acceleration data as input. When the Euclidean distance of raw acceleration data is used as a damage index or an objective function, the problem is that, for a certain Euclidean distance, the possible number of representation of raw acceleration data is infinite. In other words, the raw acceleration data will be easily affected by the appearance of noise. In our proposed methodology, STSA of raw acceleration data is a coarse graining process, an important advantage of STSA is its robustness to measurement noise. It is expected that small changes in time series data do not affect the symbolized data. Therefore, it can be assumed that a certain band of states represents similar dynamic status of a dynamic structural system, and we also should note that instead of infinite representation of Euclidean distance when using raw acceleration data as input, representation of SSH that transformed from raw acceleration will be finite.

Taking a SDOF (single-degree-of-freedom) system with the mass m, the damping c and the stiffness k under the force $F(t)$ as an example, the dynamic equation can be represented as:

$$m\ddot{x} + c\dot{x} + kx = F(t) \tag{2.10}$$

where x represents displacement of the oscillator.

By dividing both sides by the mass m, the equation of motion is modified to

$$\ddot{x} + 2\xi\omega_0\dot{x} + \omega_0^2 x = \frac{F}{m} \tag{2.11}$$

where

$\omega_0 = \sqrt{\frac{k}{m}}$: undamped natural frequency of the oscillator

$\xi = \frac{c}{c_c} = \frac{c}{2\sqrt{mk}}$: damping ratio

Appeared in the above equation, the value

$$c_c = 2\sqrt{mk} \tag{2.12}$$

is called critical damping.

$$\ddot{x} = -\omega_0^2 x - 2\xi\omega_0\dot{x} + \frac{1}{m}F \tag{2.13}$$

At the time t, $\ddot{x}_t$ can be obtained by

$$\ddot{x}_t = -\omega_0^2 x_t - 2\xi\omega_0\dot{x}_t + \frac{1}{m}F_t \tag{2.14}$$

As the window length is T, and the word length is r, all the raw acceleration data in the window is $\ddot{x} = \{\ddot{x}_0, \ddot{x}_1, \dots, \ddot{x}_{T-1}\}$. Mean value of $\ddot{x}$ is:

$$\overline{\ddot{x}} = \frac{\sum_{t=0}^{T-1}\ddot{x}_t}{T} = \frac{\sum_{t=0}^{T-1}(-\omega_0^2 x_t - 2\xi\omega_0\dot{x}_t + \frac{1}{m}F_t)}{T} \tag{2.15}$$

So far, we describe the mean value of $\ddot{x}$ of noise free case. In case the raw acceleration data we can obtain is polluted by noise, in that situation, the acceleration data at time t will be:

$$\ddot{x}_t^{'} = \ddot{x}_t + \delta_t \tag{2.16}$$

where δ_t is the value of noise at time t. The partition line (mean value of $\ddot{x}_t^{'}$) is:

$$\overline{\ddot{x}^{'}} = \frac{\sum_{t=0}^{T-1}(\ddot{x}_t + \delta_t)}{T} = \overline{\ddot{x}} + \frac{\sum_{t=0}^{T-1}\delta_t}{T} \tag{2.17}$$

For a window length T and word length r, in case T is long enough, $\sum_{t=0}^{T-1}\delta_t \approx 0$, which means that appearance of noise will not affect the value of partition line.

A random sample of SSH is predefined as SSH_a. From Equation (2.2), any other SSH (in the name of SSH_b) will have a distance with SSH_a.

Defining:

$$\Delta SSH = SSH_b - SSH_a = [\Delta SSH_0, \Delta SSH_1, \dots, \Delta SSH_{2^r-1}]$$

$$\Delta SSH_i = SSH_{b,i} - SSH_{a,i} \quad (i \in [0, 2^r - 1]) \tag{2.18}$$

where

$$\sum_{i=0}^{2^r-1} \Delta SSH_i = 0 \text{ and } \sum_{i=0}^{2^r-1} (\Delta SSH_i)^2 = \varepsilon \tag{2.19}$$

where $i \in [0, 2^r - 1]$ and $\varepsilon \geq 2$ is an even number. Since the minimum unit of change in SSH is $\frac{1}{T-r+1}$ and the dimension of SSH is 2^r, there is a possibility that not only one but many different $SSHs$ will have the same $RSSHe$ as SSH_a. This possibility occurs when Equation (2.19) is satisfied.

The minimum number of SSH_bs that have the same $RSSHe$ as SSH_a occurs when the difference between SSH_b and SSH_a is only one minimum unit; in that case, $\varepsilon = 2$, the minimum number is: $N_{min} = 2^r(2^r - 1)$. If there are two different minimum units between SSH_b and SSH_a, ε equals 4, 6 or 8. $\varepsilon = [2 * \theta, 2 * \theta + 2, \dots, 2 * \theta^2]$, where θ is the number of different units between SSH_b and SSH_a. The number of different values of ε is $N_\varepsilon = \theta^2 - \theta + 1$. For every certain value of ε can be called as a representative band, then the number of representative band is N_ε. Also, we can see that for a certain combination of $\Delta SSHs$, when α is the number of elements for which $\Delta SSH_i \neq 0$, $(i \in [0, 2^r - 1])$, the possible combinatorial number is $\binom{\alpha}{2^r}$. For

example, when $r = 9$ and α is the minimum 2, the combinatorial number is 130816, which is a big number, and we should note this is only the minimum one. The conclusion is that STSA has very good fault tolerance.

In addition, since the total number of units in SSH is $T - r + 1$, $\theta \leq T - r + 1$. For each representative band ε, there will be many representations of SSH_b; in other words, a small change in the raw acceleration data (say, due to noise) may not affect the $RSSHe$ between SSH_b and SSH_a.

2.6 Solution Range

As a coarse-graining process, the symbolization procedure can extract representative dynamic features of a structural system, but in so doing it may lose the details. However, with suitable partitioning and appropriate choice of STSA parameters, it has been observed that information necessary for accurate estimation is retained in symbol sequences (Rajagopalan et al., 2008).

Transforming raw acceleration data into SSH probably leads to a new relationship between the index (SSH) and structural parameters, which is many-to-one correspondence. If all of the candidate solutions in a solution space create the same SSH, all candidate solutions in this area are indistinguishable. We call this area "Solution range". The deviation between candidate solutions in "Solution range" and true solution brings the problem that if the solution can be reliable or not. Obviously, if the solution range is too wide, the accuracy of the proposed procedure will be affected. If the solution range is small enough, the candidate solutions in "Solution range" are close to the true solution. Thus the accuracy may be satisfactory.

Here we create the procedure for two purposes, one is to prove the existence of "Solution range", and the other one is to calculate the specific value of solution range

based on numerical simulation. Here we use the solution range of true solution as an example. The flowchart of searching the "Solution range" is shown in Figure 2.4, and a schematic plot of searching process is shown in Figure 2.5.

P is the reduction coefficient which should be larger than one. Initial candidate solution space is defined as $\Delta B_1 = [B_1^L, B_1^R] = [0.5 \times k_T, 2 \times k_T]$, where B_1^L and B_1^R are left and right boundary of the initial solution space respectively, $k_T = [k_{1,} k_2, \cdots, k_n]$, k_i $(i \in [1, n])$ is the true stiffness of each story, n is the number of stories. $k_c = [k_1^{'}, k_2^{'}, \cdots, k_n^{'}]$, $k_i^{'}$ $(i \in [1, n])$ is a randomly created candidate stiffness of each story in current candidate solution space.

The steps to find the solution range are:

(1) Using k_T as structural stiffness and create corresponding raw acceleration $\ddot{x}_T$, transforming it into state frequency $\widehat{D}_T$.

(2) In the current candidate solution space $\Delta B_i = [B_i^L, B_i^R]$ $(i \in [1, N])$, randomly generate N_c candidate solution k_c and use them to generate the corresponding raw acceleration data $\ddot{x}_{N_c}$ separately.

(3) Transforming N_c raw acceleration data into state frequencies $\widehat{D}_{N_c}$, and calculating the distance value $f(\widehat{D}_T, \widehat{D}_{N_c})$ (Equation (2.2)) between $\widehat{D}_{N_c}$ and $\widehat{D}_r$ respectively.

(4) Judging if all of the distance from step (2) equals zero (candidate solution k_c creates the same state frequency as k_T). If it is, current candidate solution space $\Delta B_N = [B_N^L, B_N^R]$ is the "solution range". If it is not, reduce the candidate solution space to $\Delta B_i = \frac{1}{P} * \Delta B_{i-1}$ $(i \geq 2)$, and repeat steps (1) and (2) until the stopping criteria be reached.

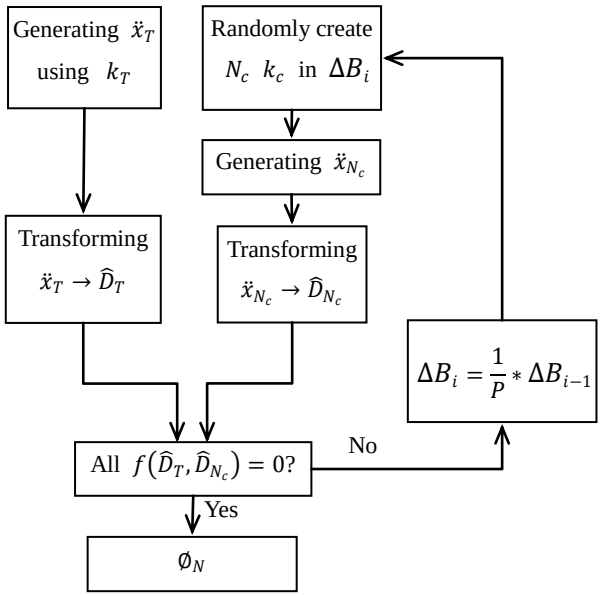

Figure 2.4. Flowchart for searching the solution range

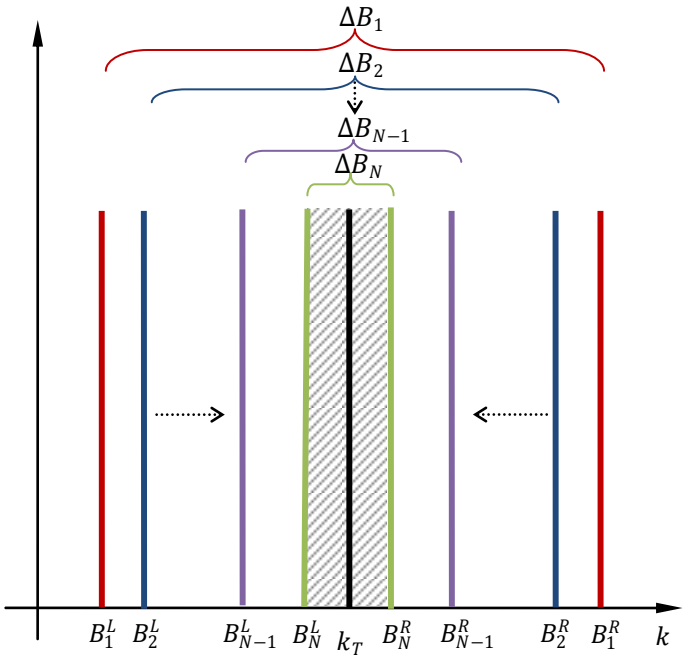

Figure 2.5. Schematic plot of solution range

2.7 Conclusions

This chapter described the main principle behind symbolic time series analysis, the detailed procedure of symbolizing raw acceleration data using different type of symbolization strategies was shown. Effect of the parameters in STSA, a window length and a word length, was explained mathematically, from the discussion we can see that a longer window length or word length responding to higher resolution of solution space, which is the foundation of obtaining acceptable results in system identification. The inter mechanisms of noise immunity by employing STSA is analyzed and the conclusion is that instead of infinite representation of the Euclidean distance when using raw acceleration data as input, representation of SSH that transformed from raw acceleration will be finite, therefore small changes in time series data do not affect the symbolized data, it can be assumed that a certain band of states represents similar dynamic status of a dynamic structural system. As doubt of the accuracy of using STSA may rise for the symbolization of raw acceleration misses some very detailed information of the original data. A novel procedure is created to verify the solution range of the system identification results, numerical verification of the procedure will be conducted in Chapter 4.

CHAPTER 3

Symbolization-Based Damage Occurrence Alarm for Building Structures

3.1 Introduction

This chapter is the first phase of the approach proposed. A symbolization-based negative selection (SNS) algorithm that combines the advantages of symbolic time series analysis (STSA) and negative selection (NS) is proposed for detecting the abnormal states of building structures. In SNS, no prior knowledge of a structure's abnormal state is needed. Only the response of the structure in a current state is used as input data. In addition, this approach works fine even with one sensor, so it is highly practical and flexible. A state sequence histogram (SSH) transformed from raw acceleration data by using STSA can capture the main features of structure dynamics and alleviate the effects of harmful noise. SSHs of the normal and abnormal states of a structure are defined as self and non-self elements, respectively. A new detector generation strategy and matching mechanism is proposed that makes the procedure

more effective, along with guidelines for appropriate parameters in SNS. Numerical simulations and experimental verifications for different abnormal state cases were conducted to demonstrate the feasibility of the proposed method.

Based on the numerical simulation for a five-story shear structure, the appropriate parameters, generality and efficacy of SNS are studied. The damage index, the relative state sequence histogram (RSSH) error, is calculated for the single structural damage, followed by double and triple damages at different damage locations. Several ground motions are used to certify the generality of this approach.

3.2 Negative Selection Algorithm

Forrest and Perelson (1994) proposed a negative selection algorithm that detects data manipulation caused by computer viruses. The basic idea was to generate a number of detectors in the complementary space and then to apply these detectors to classify new data as self or non-self. This algorithm is summarized in the following steps.

Given a shape-space U, self set S, and non-self set N, where

$$U = S \cup N \text{ and } \mathrm{S} \cap \mathrm{N} = \emptyset, \tag{3.1}$$

1) Define self as a set S of elements of length l in shape-space U.
2) Generate a set D of detectors, such that each fails to match any element in S.
3) Monitor S for changes by continually matching the detectors in D against S.

Ji and Dasgupta (2004) proposed a real-valued negative selection algorithm with

variable-sized detectors (termed V-Detector). The algorithm randomly determines the center of a detector, which must not lie within the hypersphere of a self-element. The radius is dynamically resized until the boundary of the region comes in contact with a self-element. The algorithm terminates if a predefined number of detectors are generated or a pre-determined proportion of non-self space is covered.

In a real-valued NS, self element $s = (c_s, r_s)$ has a center c_s, which is a vector in respect to different problems, and a self radius r_s, which is predefined by considering the recognition of existing self elements. Detector $d = (c_d, r_{ns})$ has a center c_d, which is usually a randomly generated vector in the representation space, and a non-self radius $r_{ns} \in R +$ (R is the set of all real numbers) that considers recognition with self elements and existing detectors in a detector set. Non-self element $ns = c_{ns}$ is defined as an abnormal features expression vector c_{ns}. Note that c_s, c_d, and c_{ns} are vectors that have the same data length.

The most important step in NS is detector generation. Two of the main methods are constant-size and variable-size. Constant-size means the radius of the detectors is constant, and variable-size means the radii of the detectors vary each other due to some predefined criterion.

As is shown in Figure 3.1, (a) is a constant-sized detector, and (b) is a variable-sized detector, and from left to right is "Detectors without overlap control," "Detectors with overlap control (overlap rate = 0)," and "Detectors with overlap control (overlap rate = a)," where $a \in [0,1]$ is a constant value. In the cases of no overlap control, it does not matter whether constant-sized or variable-sized is used, because both suffer the same problem of a low coverage rate of the non-self space because some of the detectors may completely overlap each other, which means we cannot find a proper rule to stop the generation process of detectors.

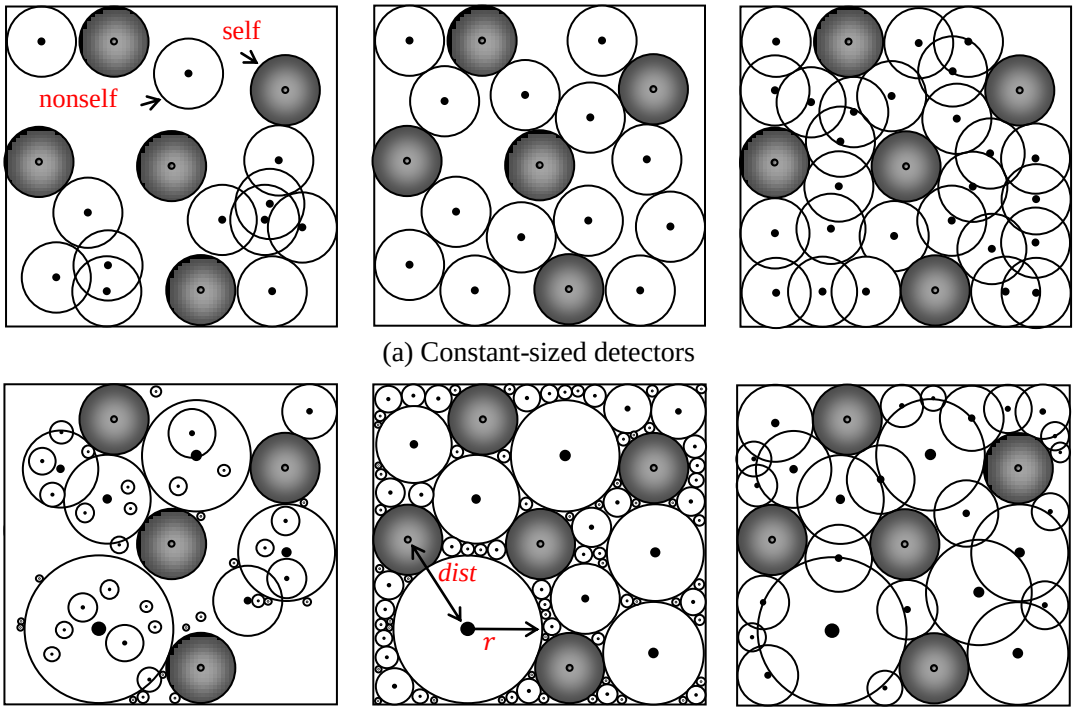

(a) Constant-sized detectors

(b) Variable-sized detectors

Figure 3.1. Comparison between constant-sized and variable-sized detectors

If the overlap rate is zero, constant-sized detectors will be uniformly distributed in the non-self space, but the coverage rate and number of detectors will be a dilemma. As a higher coverage rate is reached, a smaller radius should be chosen, which means much more detectors should be generated. For the case of variable-sized detectors, even comparing with no overlap control, a high coverage rate is obtained, and the number of detectors also increases greatly at the same time.

When the detectors are allowed to overlap each other at a proper rate, which is shown in the right figure of Figure 3.1, the constant-sized detectors will reach a much higher coverage rate with a small increase in the number of detectors. Also, for the variable-sized detectors, as a high coverage rate is maintained, the total number of detectors will be reduced greatly. Theoretically, variable-sized detectors with overlap control should be chosen.

3.3 Symbolization-Based Negative Selection Algorithm

An abnormal state detection method is proposed for building structures which called the "symbolization-based negative selection (SNS) algorithm."

In SNS, the center of a self element c_s is a SSH transformed from raw acceleration data of a structure in a current state. The center of detector c_d is a redistribution of the states of self elements. A non-self element ns is defined as a SSH transformed from raw acceleration data of a structure in an abnormal state.

Qian and Mita (2008) introduced an acceleration-based damage indicator, the relative root mean square error (RRMSe), for damage detection in building structures. The definition is shown below.

$$RRMSe = \sqrt{\frac{\sum_{t=1}^{T}\left(\ddot{x}_t^{'} - \ddot{x}_t\right)^2}{\sum_{t=1}^{T}(\ddot{x}_t)^2}} \tag{3.2}$$

where T is the number of sampling data, and $\ddot{x}_t^{'}$ and $\ddot{x}_t$ are the raw acceleration values of different acceleration segments at sampling step t.

For the proposed methodology, instead of using $RRMSe$ to measure the distance between two raw acceleration data, we use relative state sequence histogram ($RSSHe$), shown in Equation (2.2), as an index to measure the distance between two different SSH.

3.3.1 Detection Rate and False Alarm Rate

In SNS, positive is assigned as healthy and negative as abnormal. Thus, our interest

lies in how accurately the abnormal state can be detected.

To evaluate the classification accuracy in such a situation, two indexes are used. One is detection rate (DR), and the other is the false alarm rate (FAR). The DR is the ratio of negative elements correctly classified to the total negative elements, and the FAR is the ratio of positive elements incorrectly classified to the total negative elements. Four values are needed to calculate the DR and the FAR, which are the number of true positives (TP, positive elements identified as positive), true negatives (TN, negative elements identified as negative), false positives (FP, negative elements identified as positive), and false negatives (FN, positive elements identified as negative). Then, the DR and the FAR can be obtained by:

$$\mathrm{DR} = \frac{\mathrm{TN}}{\mathrm{TN}+\mathrm{FP}} \tag{3.3}$$

$$\mathrm{FAR} = \frac{\mathrm{FN}}{\mathrm{TP}+\mathrm{FN}} \tag{3.4}$$

3.3.2 Procedure of Symbolization-Based Negative Selection Algorithm

The procedure of SNS is shown in Figure 3.2, and the steps include:

1) Training phase

   a) A rectangle window with the length T is chosen and slid along the raw acceleration data series with the length L of a structure in a current state one by one to create a subseries of raw acceleration data. STSA is applied to each sub series to create a corresponding SSH_j $(j = 1,2, \dots, L - T + 1)$.

   b) When calculating the distance ($RSSHe$) between the newly created SSH with all existing SSHs in a self set, if one of the distances is less than the

predefined self radius r_s, the new SSH will be neglected. Otherwise, store it in the self set as a new self element. Repeat this procedure until the predefined criteria is satisfied.

c) Apply NS to the self set to generate detectors.

2) Detecting phase

a) For the newly encountered raw acceleration data of a structure, when symbolizing it by using the same method in step a) of the training phase, a corresponding $\widehat{SSH}_j$ will be generated.

b) When matching $\widehat{SSH}_j$ with the detectors generated in the training phase, if any detectors are activated (distance between them is less than a certain value), a signal indicating the occurrence of the abnormal state of a structure will be given.

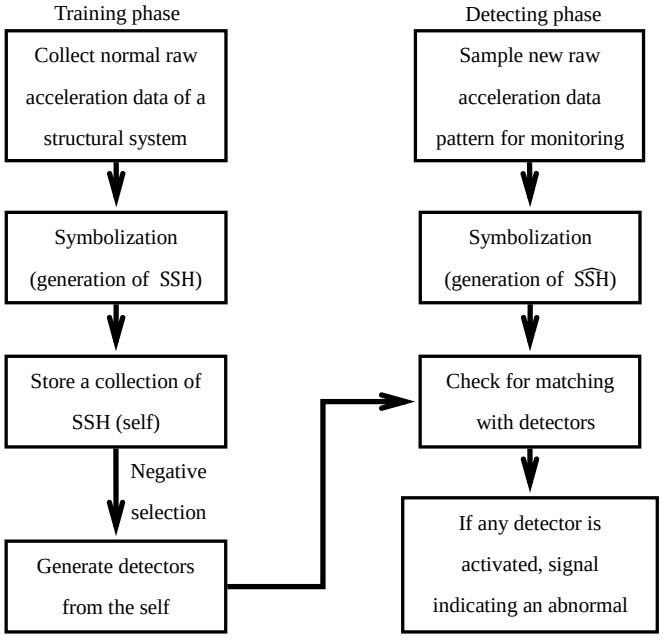

Figure 3.2. Schematic diagram showing the processing stage of SNS

3.3.3 Procedure of Detector Generation

Basically, supposing that SSH can capture the dynamic features of a structure, the abnormal state of the structure will be expressed by other distributions of states in a SSH. Instead of randomly generating candidate detectors (which may result in creating an impossible distribution of states in the SSH), a novel procedure to create candidate detectors on the basis of self elements is proposed. The procedure is shown below.

1) Redistribution: Randomly choose n (integer $n \in [2, 2^r]$) states from SSH_j ($j \in [1, N_s]$) and keep the rest unchanged, where N_s is the number of self elements. Randomly redistribute the frequency value of n chosen states and keep the sum of them unchanged. Note that the minimum unit to change is $\frac{1}{T-r+1}$.

2) Self recognition: Calculate the distance between candidate detectors and all $SSHs$ in the self set. If the minimum distance $dist_s < r_s$ (r_s is the self radius), delete it. If not, keep it for the next step.

3) Existing detectors recognition: Calculate the distance between the candidate detector and existing detectors. If the minimum distance $dist_d < r_d * (1 - r_o)$ (r_d is the radius of existing detectors; r_o is the overlap rate, defined in 3.3.4), delete it. If not, store it as a new detector. Set $dist_d$ as the radius of the new detector.

4) Repeat steps 1) ~ 3) until the predefined stopping criterion is satisfied.

3.3.4 Self Radius

In SNS, the main control parameters include two classes. One is the control parameters of STSA, which include the window length T and the word length r (mathematically described in Section 2.4). The other class includes parameters that may affect the performance of NS, which are the coverage rate c_r, the self radius r_s, the overlap rate r_o, and the size of the detector set N_d.

For the coverage rate (Ji and Dasgupta, 2004), when randomly sampling one point in the considered space m times without finding a point uncovered by the detectors, the coverage rate of non-self space would be $c_r = 1 - \frac{1}{m}$. For the overlap rate (Chen and Liang, 2008), $r_o = 1 - \frac{d'}{R' + r'}$, d' is the distance between two points, and R' and r' are respectively their radii.

Referring to the previous research work (Forrest and Perelson, 1994; Chen and Liang, 2008), the coverage rate and the overlap rate are set to be 99.8% and 25%, respectively, and the size of detector set N_d is preset to be the maximum allowable in practice that does not need much more consideration. This size is 3.0×10^4. The effect of the window length, the word length, and the self radius on the performance of SNS needs to be verified.

The self radius r_s is an important factor for balancing the DR and the FAR; in other words, the sensitivity and accuracy of NS. First, r_s should be chosen as a value larger than $RSSHe_{dis}^{min}$,

$$r_s > RSSHe_{dis}^{min} \tag{3.5}$$

If r_s is too small, all SSHs will be collected into the self set. In that case, although a

high DR can be obtained, the FAR will be high, for there is no possibility of creating a complete self set.

If r_s is too big, only a few self elements will be created because all the other $SSHs$ from the structure in a normal state will be recognized by the existing self elements and will be deleted. If that is the case, although a low FAR can be obtained since the whole self space can be covered, note that part of the non-self space will also be covered by the self elements, which will result in a low DR.

Suppose normal SSHs from a healthy structure have been collected, which is ($SSH_1, SSH_2, \dots, SSH_n$). Then, ($RSSHe_{dis}^1, RSSHe_{dis}^2, \dots, RSSHe_{dis}^n$) can be calculated for each SSH by using Equation (2.5). For simplicity, we recommend choosing a self radius a little higher than $max(RSSHe_{dis}^i), i \in [1, n]$.

As mathematically explained in Section 2.4, a bigger value for the window length and the word length is related to a higher resolution, which means that the self and the non-self spaces can be separated much more accurately. This is the foundation for obtaining a high DR and a low FAR. The minimum value for the window length and the word length to obtain acceptable performance should be decided according to DR and FAR analyses for the target problem.

In the field of detecting the abnormal states of building structures, due to a series of simulations (Section 3.4), the word length r and the window length T are recommend as:

$$r \geq 9 \text{ and } T \geq \frac{60}{f_{1st}} * f_s \tag{3.6}$$

where f_{1st} is the fundamental natural frequency of the structure and f_s is the sampling frequency.

3.4 Numerical Simulation

In this section, the main parameters of SNS are chosen, and the effects of them are examined. The different abnormal states of a structure are considered to be stiffness reduction with different locations and degrees to show the generality of SNS. Also the performance of SNS is compared with existing methods such as the artificial neural network (ANN) (Bakhary et al., 2007; Qian and Mita, 2008) and support vector machine (SVM) (Mita and Hagiwara, 2003; Cho et al., 2005) to show the effectiveness of our proposed method.

3.4.1 Examined Parameters

A five-story shear frame structure was used for simplicity and generality, and it was modeled as a multiple degree-of-freedom lumped mass system (Figure 3.3). Structural parameters and modal parameters are shown in Table 3.1. The dynamic equation is (Mita, 2003):

$$M\ddot{X}_t + C\dot{X}_t + KX_t = f(t) \tag{3.7}$$

where M, C, and K are respectively the mass, damping, and stiffness matrices. $f(t)$ is the force vector linked to the ground acceleration. The vectors $\ddot{X}$, $\dot{X}$, and X are respectively relative acceleration, velocity, and displacement responses. The damping ratios of each story was set to 0.03. The sampling frequency was 100 Hz. In training phase, Gaussian white noise is used as input signal, in detecting phase, synthetic earthquake is used as input signal, an example of the synthetic earthquake is shown in Figure 3.4.

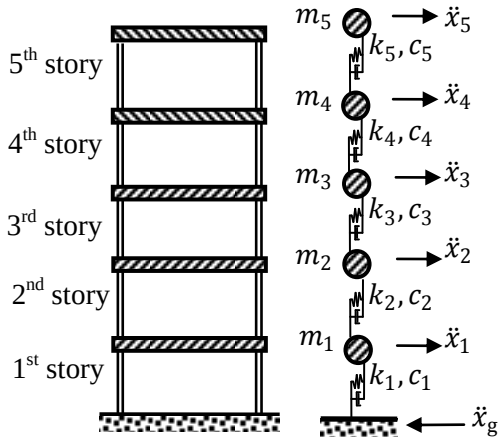

Figure 3.3. Five-story shear frame structure

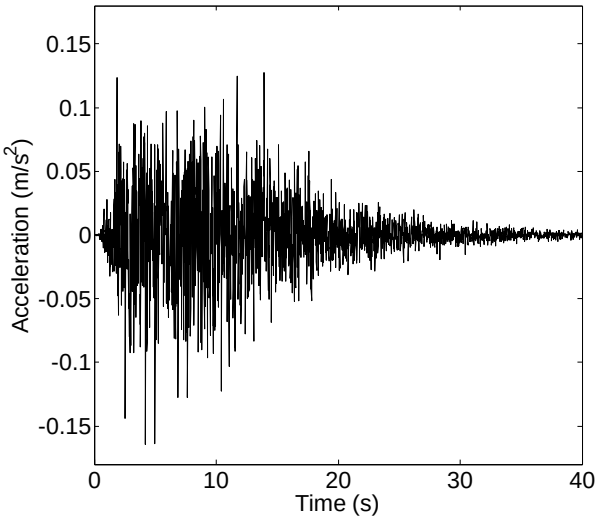

Figure 3.4. Example of synthetic earthquake

Table 3.1. Structural and modal parameters of the structure

Mode number	1	2	3	4	5
Mass (kg)	1000	1000	1000	1000	1000
Stiffness ($\times 10^6$N/m)	2.00	2.00	2.00	2.00	2.00
Frequency (Hz)	2.03	5.91	9.32	11.98	13.66

To eliminate the effect of the input signal, $RSSHe$ among the normal SSHs (gotten by symbolizing raw acceleration of the 5th story of the structure at normal state) is calculated 100 times independently by using randomly generated ground motions (L=2×10^4) each time. Also, the variation of stiffness of each story in a practical problem was simulated as a $\pm$1% deviation of the original one. This factor was considered by choosing the stiffness of each story in this deviation range randomly in each case. The window length and the word length was 3.0×10^3 and 9, respectively. The number of normal SSHs was 1.0×10^4 in each case. The range of $RSSHe$ of the normal SSHs for all the case is shown in Figure 3.5. The top of the box is the maximum value, the bottom of the box is the minimum value, and the short line in each box means the value.

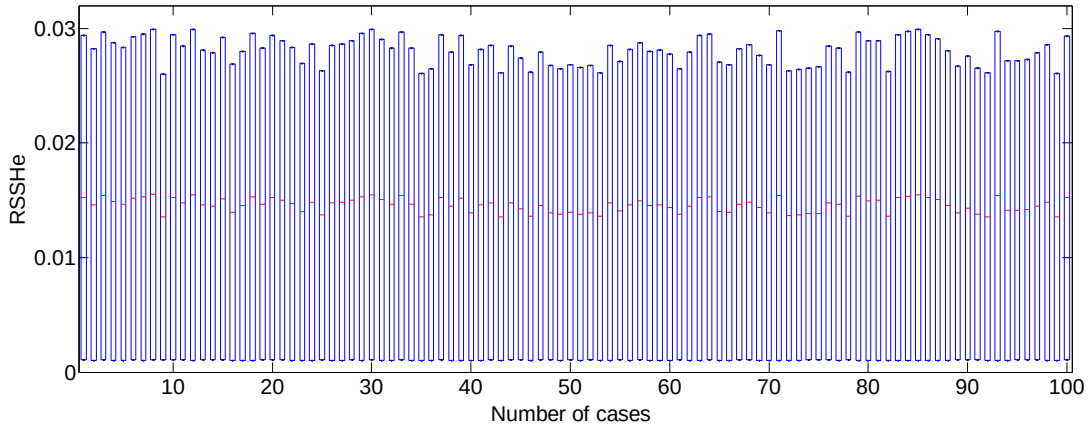

Figure 3.5. RSSHe of self elements

From the results, the ranges of $RSSHe$ found by using different ground motions were all around 0.001 to 0.03. The self radius r_s should be an appropriate value in this range. Then, the abnormal state of the structure was modeled by reducing the stiffness by 20% at the first story. The testing data set for SNS included 1.0×10^3 SSHs from the structure in the current and abnormal states, respectively. Figures 3.6 and 3.7 show the complete trends of the self radius' effect on the results for self radii that varied

from 0.001 up to 0.03. This includes the relationship between radius r_s and the DR, the FAR, the size of self set, and also the size of detector set.

From Figure 3.6, as the value of self radius increase, DR and FAR will decrease simultaneously. From Figure 3.7, The bigger the self radius, the less the self elements.

The size of detector set will also change due to different self radius.

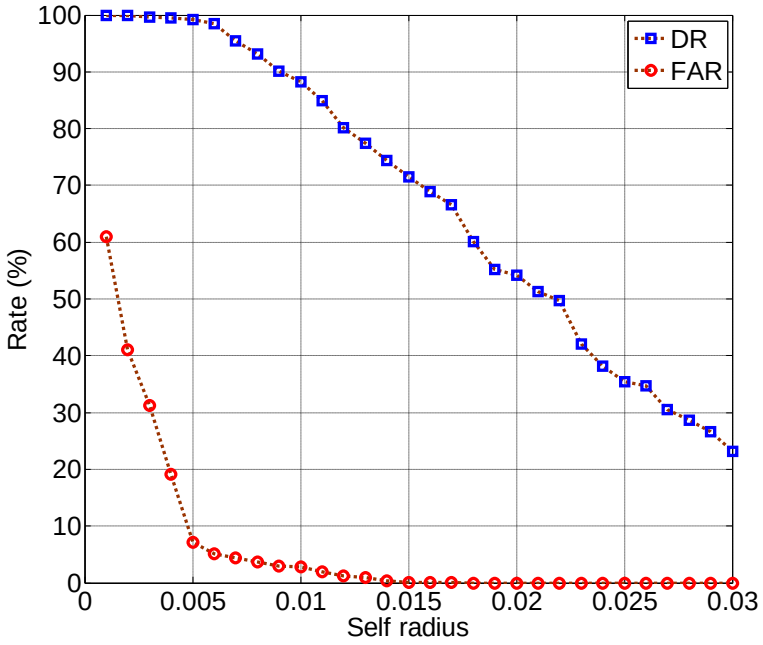

Figure 3.6. Relationship between self radius and DR/FAR

To balance the performance of different aspects, 0.005 seemed to be an appropriate value for the self radius, and it also fits Equation (3.5) as $r_s > \frac{\sqrt{2}}{T-r+1} = 4.73 \times 10^{-4}$.

As stated before, the window length and the word length are the control parameters of the STSA. Here, 0.005 was chosen as the self radius. The first simulation was that the word length varied from 3 to 12 keeping the window length as 3000. The second simulation was to choose 9 as the word length varying the window length from 1000 to 4000 at intervals of 500. The results are shown in Figures 3.8 and 3.9, respectively.

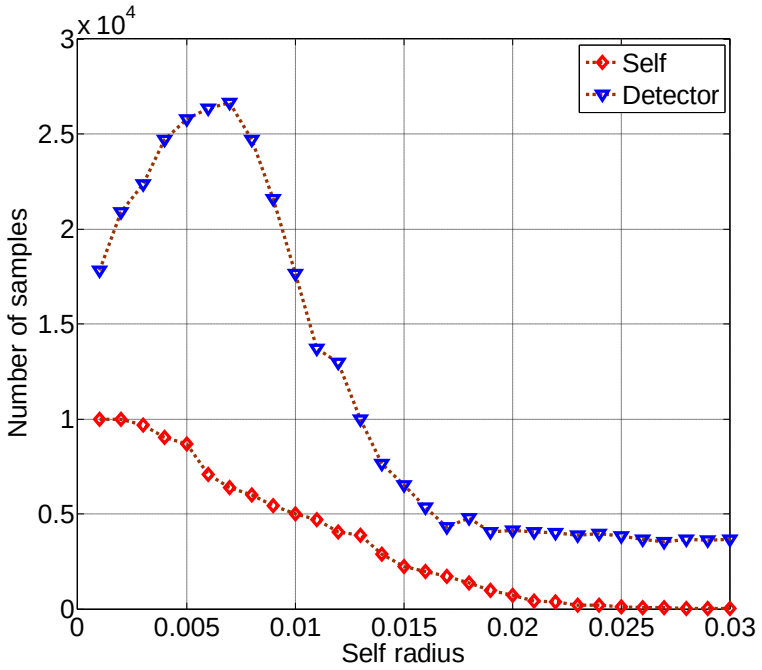

Figure 3.7. Relationship between self radius and size of self and detector set

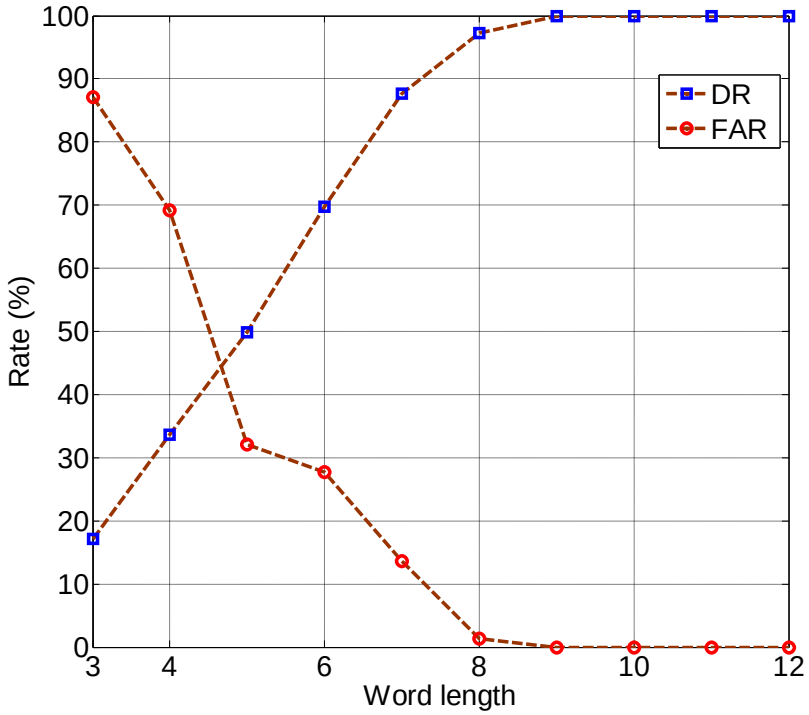

Figure 3.8. DR/FAR of different word lengths (T = 3000)

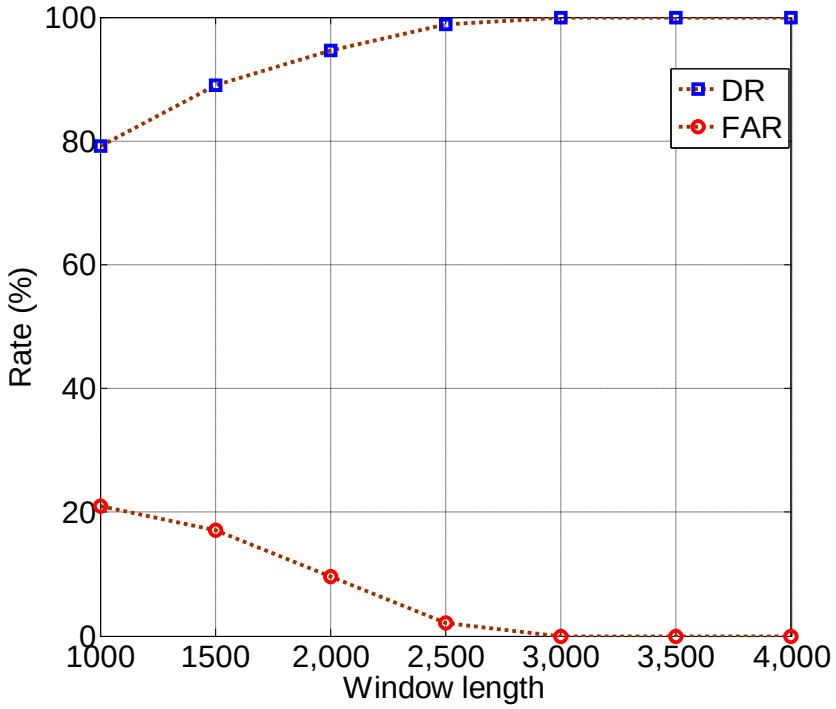

Figure 3.9. DR/FAR of different window lengths (r = 9)

Figure 3.8 and Figure 3.9 indicate that the word length and the window length greatly affected the performance of SNS. A larger word length and window length gave better performance. The reason is that a larger word length and window length can symbolize the raw acceleration data much more accurately than a shorter one. As more dynamic information of the system was captured, the detection rate increased, and the false alarm rate decreased simultaneously. In the simulation, even a word length of 9 to 12 or a window length more than 3000 gave the same best result (DR = 100%; FAR = 0), and the calculating complexity when 12 as the word length or 5000 as the window length was chosen increased greater than that when 9 and 3000 were chosen. To balance the cost of the computation source and efficiency of the method, a word length of at least 9 and a window length of 3000 are recommend.

As the sampling frequency in these simulations was set as 100Hz, 9 as word length

and 3000 as window length may be suitable, but there is possibility that different sampling frequency may results in different appropriate value of window length or word length. Same simulation as previous was conducted but the sampling frequency was set as 150Hz. The results was shown in Figure 3.10. By verifying the damage detection results with bigger word length and window length, the appropriate word length and window length for this case providing perfect results (DR = 100%; FAR = 0) are 11 and 5000, respectively.

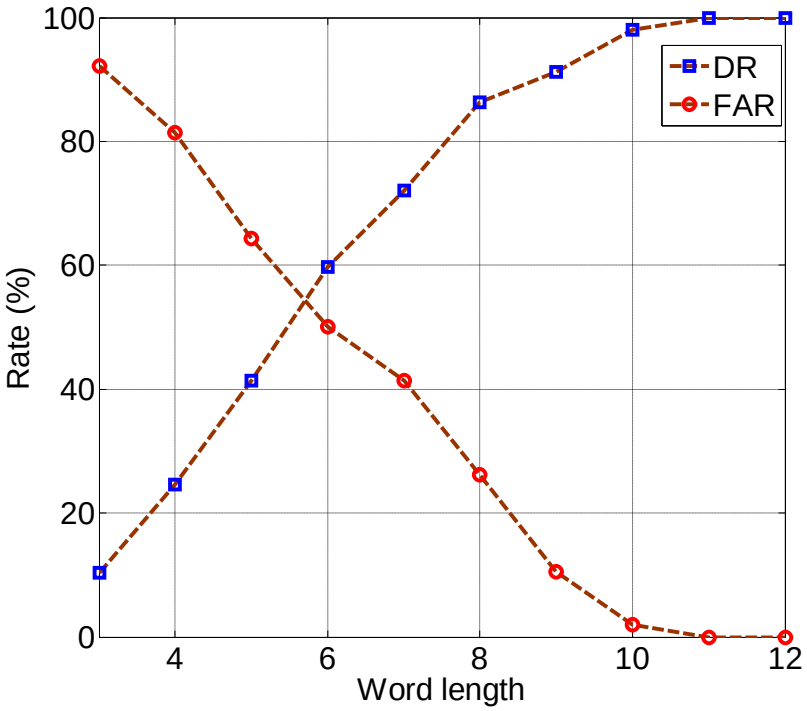

Figure 3.10. DR/FAR of different word lengths (T = 5000)

The following are a few qualitative observations on appropriate window and word lengths with a given sampling frequency. The increased lengths of word and window are suitable as the sampling frequency becomes higher. If the sampling frequency is too low, the information contained in original signal will be missed. In that case, the

generated SSH cannot be considered as index that can capture the dynamic features of structures. If the sampling frequency is too high, window length need to be bigger to contain enough dynamic information of the structure, and also the symbol series that transformed from raw acceleration data will contain a large number of continuous same symbols, which need a bigger word length to generate word. As we explained before, bigger word length related to a higher dimension of SSH, which also means a much more complex solution space, which will affect the effectiveness of the proposed method.

3.4.2 Different Abnormal States

Several tests were performed according to the different abnormal states of the structure by simulating stiffness reduction at different locations and degrees. Moreover, some noise (1%, 5%, and 10%) was added to the acceleration response. Abnormal states included stiffness reduction at one story (1st story), two stories (1st and 3rd story), and three stories (1st, 3rd, and 5th story). Degrees included 5%, 10%, and 20% stiffness reduction.

The results are presented below in Table 3.2. A comparison of the DR and FAR for different abnormal states is shown in Figures 3.11 to 3.13.

The results show that, a high DR and low FAR can be obtained no matter the locations and degrees of stiffness reduction. The noise addition is not problematic for damage detection though the noise level increases and the detection rate decreases, but the extent of increase of FAR or decrease of DR is very small. Indeed, acceptable results can be obtained probably due to the fact that the $RSSHe$ is much more sensitive to changes in the structure itself than to the environment (appearance of noise).

Table 3.2. DR and FAR of different abnormal states (T = 3000 and r = 9)

Noise level (%)	Number of stiffness reduced stories								
	One			Two			Three		
	Location & Degree	Rate (%) DR	Rate (%) FAR	Location & Degree	Rate (%) DR	Rate (%) FAR	Location & Degree	Rate (%) DR	Rate (%) FAR
0	1st&5%	100	0	1st&5% 3rd&5%	99.90	0.00	1st&5%	99.98	0.00
1		99.77	0.04		99.28	0.02	3rd&5%	99.77	0.03
5		98.56	0.05		99.04	0.06	5th&5%	99.17	0.14
10		97.78	0.48		98.31	0.21		99.06	0.44
0	1st&10%	100	0	1st&10% 3rd&10%	99.97	0.00	1st&10%	99.98	0.00
1		99.68	0.13		99.77	0.11	3rd&10%	99.82	0.11
5		98.57	0.28		99.14	0.17	5th&10%	99.54	0.18
10		97.89	0.50		98.80	0.31		98.79	0.45
0	1st&20%	100	0	1st&20% 3rd&20%	100.00	0.00	1st&20%	100.00	0.00
1		99.90	0.06		99.92	0.09	3rd&20%	99.90	0.09
5		99.05	0.03		99.66	0.13	5th&20%	99.67	0.17
10		98.15	0.08		98.79	0.29		98.89	0.39
0	5th&5%	100	0	1st&5% 3rd&10%	99.95	0.00	1st&5%	99.98	0.00
1		99.71	0.03		99.59	0.08	3rd&10%	99.88	0.16
5		98.67	0.04		99.50	0.11	5th&20%	99.37	0.21
10		96.03	0.51		98.29	0.39		98.71	0.49
0	5th&10%	100	0	1st&5% 3rd&20%	100.00	0.00	1st&10%	99.98	0.00
1		99.91	0.01		99.79	0.04	3rd&10%	99.92	0.12
5		98.83	0.17		99.20	0.05	5th&20%	99.27	0.20
10		98.01	0.21		99.10	0.16		98.00	0.35
0	5th&20%	100	0	1st&10% 3rd&20%	100.00	0.00	1st&10%	100.00	0.00
1		99.97	0.01		99.84	0.06	3rd&20%	99.87	0.13
5		99.15	0.09		99.61	0.18	5th&20%	99.01	0.21
10		98.07	0.12		98.99	0.29		98.64	0.47

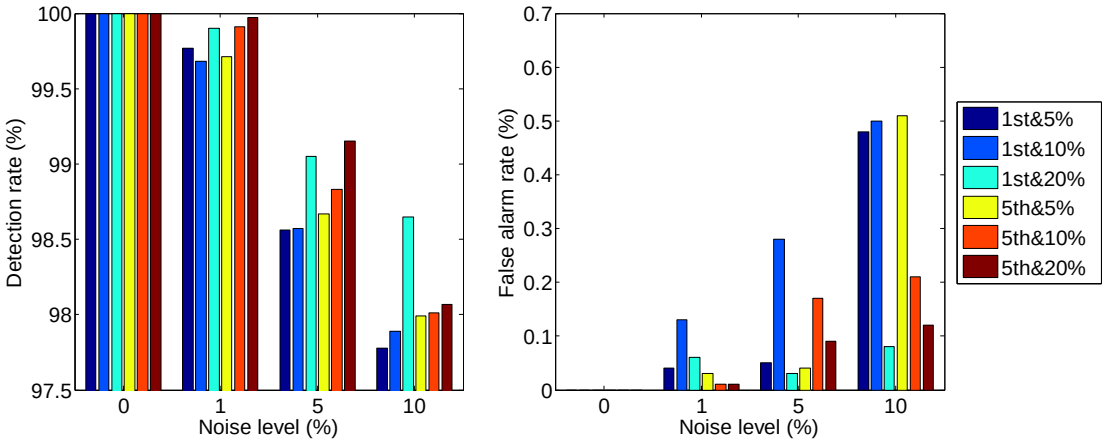

Figure 3.11. DR and FAR for one-story case (damage at 1st/5th story, T = 3000 and r = 9)

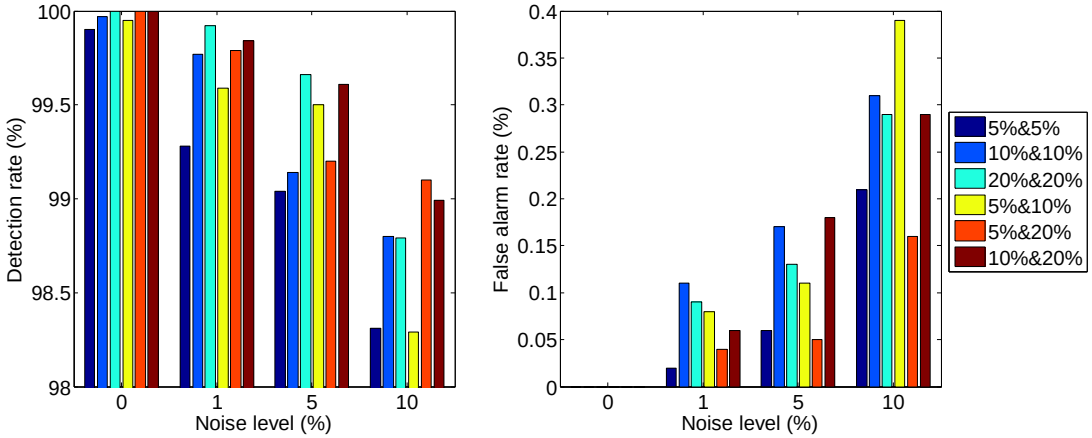

Figure 3.12. DR and FAR for two-story case (damage at 1st and 3rd story, T = 3000 and r = 9)

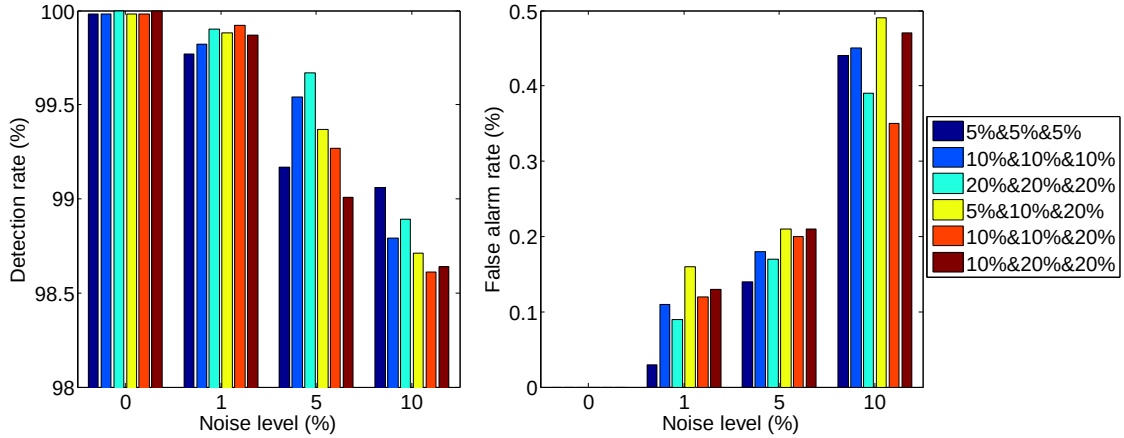

Figure 3.13. DR and FAR for three-story case (damage at 1st, 3rd and 5th story, T = 3000 and r = 9)

3.4.3 Comparison with Artificial Neural Network and Support Vector Machine

Artificial neural network (ANN) (Qian and Mita, 2008) and support vector machine (SVM) (Mita and Hagiwara, 2003) were used for comparisons to show the effectiveness of SNS. In SNS, constant-sized detector (SNS(C)) and variable-sized detector (SNS(V)) generation strategies are calculated separately. In ANN and SVM, all SSHs from a data set (include normal and abnormal) are used to train the models of the ANN or SVM, while only normal SSHs is used to create detectors in SNS. The number of normal SSHs in training phase is 1.0×10^4; the number of normal or abnormal SSHs in examination data set is 1×10^3, respectively.

The ANN used in this experiment was implemented by using Matlab 7.1 Neural Network Toolbox software. The Levenberg-Marquardt algorithm (Lera and Pinzolas, 2002) was also used. A standard three-layer network was chosen. In the input layer, there were 124 nodes, equal to the number of system calls. The number of output nodes was equal to 1. On the basis of tests, we determined that the ANN with seven hidden nodes achieved the best performance.

In our test using the SVM, we chose the Gaussian kernel as our kernel function because it tends to achieve better performance. The parameters that must be determined are the kernel bandwidth and the margin, which were determined to be 2 and 10, respectively.

The results show that SNS(V) gave the best results in both the noise free and noise polluted cases. Usually, the DR will decrease and the FAR will increase as the noise level increases. For example, when the noise level is 10%, the best result is given by using SNS(V), and the DR is 100%, and the FAR is 1.64%, while the results for the DR and FAR by using the ANN are 93.22% and 5.99%, respectively, which is worse than using SNS(V).

The results of using SNS(C), SNS(V), ANN, and SVM are shown in Table 3.3.

Table 3.3. Comparison among SNS(C), SNS(V), ANN, and SVM

Noise level	SNS (C)		SNS (V)		ANN		SVM	
	DR	FAR	DR	FAR	DR	FAR	DR	FAR
0	97.20	0.92	**100**	**0.00**	99.51	1.26	96.58	9.04
1%	95.13	1.31	**100**	**0.00**	97.00	2.02	91.89	10.71
5%	94.00	3.13	**99.88**	**1.36**	96.19	3.51	87.97	15.78
10%	92.31	5.13	**98.47**	**1.64**	93.22	5.99	77.88	25.22

The comparison between SNS(C) and SNS(V) indicates that the strategy of using variable-sized detectors can cover the non-self space much more effectively than that using constant-sized detectors.

As declared before, based on the basic fact that the distribution of states in a SSH will always follow a rule (Section 3.3.3), randomly generated candidate detectors cannot generate detectors effectively. A methodology is proposed to generate the candidate detector. The effect should be proved through comparison with the strategy of randomly creating candidate detectors. In case of using a noise free signal, the proposed methodology resulted in a DR equal to 100% and an FAR equal to 0, while the random one resulted in a DR equal to 56.94% and a FAR equal to 38.87%. It can be said that the self and the non-self cannot be classified correctly by using the random methodology.

3.5 Conclusions

In this chapter, we proposed a symbolization-based negative selection algorithm that merges the merits of STSA and NS for abnormal state detection of building structures. Using STSA alleviated harmful noise. In SNS, the benefit of using NS is that only

knowledge of a structure in a current state is needed. The main components of NS and the corresponding strategy of generating detectors were defined. A procedure for determining the control parameters of SNS was presented. The effectiveness of the proposed method was well verified by performing numerical simulation and experimental verification for five-story shear structure models. Comparison with existing methods such as the ANN and SVM showed that SNS was indeed a powerful tool for abnormal state detection of building structures.

CHAPTER 4

Symbolization-Based Damage Localization and Quantification of Structures

4.1 Introduction

This chapter is the second phase of the proposed approach. After knowing the damage occurrence, the next phase is necessary to be performed for the goal of determining the damage location and quantity. Most of currently available damage localization approaches are based on pattern recognition methods to classify the different damage location. However, such approaches need analytical data for all damage case situations, which can be computationally expensive and even impossible. Therefore, the system identification is utilized for damage determination. In this research the system identification problem is formulated as an optimization problem using the Differential Evolution (DE) strategy.

Based on the numerical simulations for a five-story shear frame structure, the performance of this method is studied for both full output information and partial output information. Moreover the advantage of this method is verified by comparison with the other global search methods, e.g. DE and Particle Swarm Optimization (PSO) using raw acceleration data.

4.2 System Identification as an Optimization Problem

The identification problem can be understood as an optimization problem in which the error between the actual physical measured response of a structure and the simulated response of a numerical model is minimized. In order to show this in more detail, let us consider a physical system as shown in Figure 3.3 with q outputs of acceleration responses y_j^M for $j = 1,2,\dots,q$. Let y_j^M for $j = 1,2,\dots,q$ denotes the value of the acceleration responses of the actual system.

Suppose that a model that is able to capture the behavior of the physical system is developed and that this model depends upon a set of n parameters, contained in a vector $x = \{x_i\}$ for $i = 1,2,\dots,n$. Call the newly formed model of the system and its parameters the identified system or candidate system, and let y_j for $j = 1,2,\dots,q$ denotes the value of the acceleration responses of the identified system. *T* is the final time step. At this point, let us now build the vectors y_j^M and y_j as

$$y_j^M = \left[y_j^M(0)\ \ y_j^M(1)\ \ \dots\ \ y_j^M(T)\right], \quad j = 1,2,\dots,q \tag{4.1}$$

$$y_j = \left[y_j(0)\ \ y_j(1)\ \ \dots\ \ y_j(T)\right], \quad j = 1,2,\dots,q \tag{4.2}$$

containing all sampled values of the *j*th output of the actual and the identified systems, respectively. Now consider the vectors y_j^M and y_j, as the stacked vectors of all available output records for each system, which can be written as

$$y^M = \left[y_1^M(0)\ y_1^M(1)\ \ \dots\ y_1^M(T)|y_2^M(0)\ \ \dots|\dots|y_q^M(0)\ \ \dots\ y_q^M(T)\right] \tag{4.3}$$

$$y = [y_1(0)\ y_1(1)\ \ \ldots\ y_1(T)|y_2(0)\ \ \ldots|\ldots|y_q(0)\ \ \ldots\ y_q(T)] \tag{4.4}$$

and compute the error norm of all the simulated outputs of the identified system with respect to those measured from the actual system, defined as:

$$F(x) = \sqrt{(y^M - y)(y^M - y)^T} \tag{4.5}$$

In order to obtain a successful identification, the candidate system must be able to accurately reproduce the output of the physical system for any given input. Therefore, our interest lies in minimizing the error norm of the outputs. Formally, the optimization problem requires finding a vector $x \in S$, where S is the search space, so that a certain quality criterion is satisfied, namely that the error norm $F: S \to R$ is minimized. The function F is commonly called a cost function or objective function. In evolutionary computation, typically a fitness function is used which reflects the goodness of the solution. The better the solution, the fitter it is for survival. As our problem is a minimization problem, a fitter solution will be characterized with a lower value of the cost function. Therefore, the fitness function can be defined as the negative of the cost function, i.e., $-F$. Minimization of F is then equivalent to maximize the fitness $-F$. Vector x^* will be called a solution to the minimization problem if $F(x^*)$ is the global minimum of F in S, or

$$x^* \in S|F(x^*) \leq F(x) \quad \forall x \in S \tag{4.6}$$

The search space S is defined by a set of the maximum and the minimum values for each parameter. It is conceived as an n-dimensional domain delimited by vectors $x_{\max}$ and $x_{\min}$ containing the upper bounds of the n parameters and the lower bounds respectively or

$$\mathrm{S} = \{\text{space} \quad x \in R^n \left| x_{min,i} \le x_i \le x_{max,i} \right. \quad \forall i = 1,2,\dots,n\} \tag{4.7}$$

The problem of identification is thus treated as a linearly constrained (due to the delimited n-dimensional search space) nonlinear (due to the nonlinear cost function) optimization problem.

4.3 Differential Evolution Strategy

The DE algorithm (Storn and Price 1996, Price and Storn 1997) is a population based algorithm like genetic algorithms using the similar operators: crossover, mutation and selection. In DE, a population of N_P (population size) solution vectors is initialized randomly at the start, which is evolved to find optimal solutions through the mutation, crossover, and selecting operation procedures.

Differential evolution (DE) resembles the structure of an evolutionary algorithm (EA), but differs from traditional EAs in its generation of new candidate solutions and by its use of a 'greedy' selection scheme. Another main characteristic of DE is with its ability to search with floating point representation instead of binary representation that is being used in many basic EAs. DE is one such hybrid, taking the concepts of 'larger populations' from genetic algorithms, and 'self-adapting mutation' from evolutionary strategies. The characteristics together with other factors of DE make it a fast and robust algorithm as an alternative to EA (Tang et al., 2008).

The detailed steps of DE (Tang et al., 2008) are described as below.

An optimization task consisting of n parameters can be represented by an n-dimensional vector. Let $S \in R^n$ be the search space of the problem under consideration. Then, the DE algorithm utilizes N_P, n-dimensional vectors

$$x_i = (x_{i1}, x_{i2}, \dots, x_{in})^{\mathrm{T}} \in S, \quad i = 1,2, \dots, N_P \tag{4.8}$$

as a population for each iteration, called a generation of the algorithm.

4.3.1 Mutation

The objective of mutation is to enable search diversity in the parameter space as well as to direct the existing object vectors with suitable amount of parameter variation in a way which will lead to better results at a suitable time. It keeps the search robust and explores new areas in the search domain.

According to the mutation operator, for each individual, $x_i^{(G)}$, $i = 1,2, \dots, N_P$, at generation *G*, a mutation vector $v_i^{(G+1)} = (v_{i1}^{(G+1)}, v_{i2}^{(G+1)}, \dots, v_{in}^{(G+1)})^{\mathrm{T}}$ is determined using one of the following equations (Storn and Price, 1997):

$$v_i^{(G+1)} = x_{r1}^{(G)} + E(x_{r2}^{(G)} - x_{r3}^{(G)}) \tag{4.9}$$

$$v_i^{(G+1)} = x_{best}^{(G)} + E(x_{r1}^{(G)} - x_{r2}^{(G)}) \tag{4.10}$$

$$v_i^{(G+1)} = x_i^{(G)} + E_1\left(x_{best}^{(G)} - x_i^{(G)}\right) + E(x_{r1}^{(G)} - x_{r2}^{(G)}) \tag{4.11}$$

$$v_i^{(G+1)} = x_{best}^{(G)} + E_1\left(x_{r1}^{(G)} - x_{r2}^{(G)}\right) + E(x_{r3}^{(G)} - x_{r4}^{(G)}) \tag{4.12}$$

$$v_i^{(G+1)} = x_{r1}^{(G)} + E_1\left(x_{r2}^{(G)} - x_{r3}^{(G)}\right) + E(x_{r4}^{(G)} - x_{r5}^{(G)}) \tag{4.13}$$

where $x_{best}^{(G)}$ represents the best individual of the population at generation *G*; E and

$E_1 > 0$ denote real parameters, called mutation constants, which control the amplification of difference between two individuals so as to avoid search stagnation; and r_1, r_2, r_3, r_4 and r_5, are mutually different integers, randomly selected from the set $\{i = 1,2,\dots,i-1,i+1,\dots,N_P\}$.

Here the choice of Equations (4.9) to (4.13) leads to different variants of DE, such as DE/rand/1/bin, DE/best/1/bin, DE/current-to-best/1/bin, DE/best/2/bin, and DE/rand/2/bin, respectively. In this study we use the DE/current-to-best/bin scheme (Equation 4.11).

4.3.2 Crossover

Following the mutation phase, the crossover operator is applied on the population. For each mutant vector, $v_i^{(G+1)}$, a trial vector $u_i^{(G+1)} = (u_{i1}^{(G+1)}, u_{i2}^{(G+1)}, \dots, u_{in}^{(G+1)})^{\mathrm{T}}$ is generated, with

$$u_{ij}^{(G+1)} = \begin{cases} v_{ij}^{(G+1)} & \text{if } (\mathrm{rand}(j) \le C_R) \text{ or } (j = \mathrm{randn}\,(i)) \\ x_{ij}^{(G)} & \text{if } (\mathrm{rand}(j) > C_R) \text{ or } (j \ne \mathrm{randn}\,(i)) \end{cases} \tag{4.14}$$

where $j = 1,2,\dots,n$; $\mathrm{rand}(j)$ is the jth independent random number uniformly distributed in the range of [0, 1], and $\mathrm{randn}(i)$ is a randomly chosen index from the set $\{1,2,\dots,n\}$, and C_R is user defined crossover constant $\in [0,1]$ that controls the diversity of the population (Storn and Price, 1997).

4.3.3 Selection

After producing the offspring, the performance of the offspring vector and its parent is compared and the better one is selected. If the parent is still better, it is retained in the population. DE employs a greedy selection process that the better one of new offspring and its parent wins the competition providing significant advantage of

converging performance over genetic algorithms.

To decide whether the vector $u_i^{(G+1)}$ should be a member of the population of the next generation, it is compared to the corresponding vector $x_i^{(G)}$. Thus, if f denotes the objective function under consideration, then

$$x_i^{(G+1)} = \begin{cases} u_i^{(G+1)} & \text{if} \quad f\left(u_i^{(G+1)}\right) > f\left(x_i^{(G)}\right) \\ x_i^{(G)} & \text{otherwise} \end{cases} \tag{4.15}$$

Thus, each individual of the trial vector is compared with its parent vector and the better one is passed to the next generation, so the best individuals in the population are preserved. These steps are repeated until specified termination criterion is reached.

4.3.4 Operational Parameters

DE has three key parameters: scaling factor of the difference vector, E, crossover control parameter, C_R and population size, N_P. An additional control variable, E_1, is introduced in DE/current-to-best/bin scheme. The idea behind the additional control variable E_1 is to provide a means to enhance the greediness of the scheme by incorporating the current best vector $x_{best}^{(G)}$. The operational parameters control the balance between exploitation and exploration. Proper configuration of the above parameters would achieve good tradeoff between the global exploration and the local exploitation so as to increase the convergence velocity and robustness of the search process. Depending on the problem and available computational resources, the population size can be in the range as low as $2n$ (n is the problem dimension) to as high as $100\,n$ (Price, 1999). Generally, with a population size of $20\,n$, $E_1 = 0.95$ and $E = 0.8$ appear to be reasonably good value to generate satisfactory results. The test results in (Storn and Price, 1997) show that a satisfactory range of C_R appears to be within 0.8-1.0.

4.3.5 Feasible Possible Parameter Space

Theoretically speaking, the search of DE for an optimum in the feasible search space S could be carried out like the other stochastic search optimization algorithms. However, in structural system identification using dynamic analysis, not all sets of parameters in the specified search space might provide physically plausible solutions to the problem. Restricting the search space to the feasible region might be difficult because the constraints are not simple (Franco et al., 2004). In this paper, a penalty strategy (Koziel and Michalewicz, 1999; Franco et al., 2004) is implemented in the DE algorithm to tackle this problem. If a candidate parameter set is not a physically plausible solution, that is the system is unstable, then an exaggerated cost function value is returned. As this value is uncommonly large in comparison to usual cost function values, these "unstable" offspring are usually eliminated in a single generation.

4.3.6 Implementation of Differential Evolution

The procedure of DE methodology can be summarized in the following steps.

Step 1: Input the required DE parameters. Initialize the population of individual for DE, randomly in the limits of specified decision variables.

Step 2: Check all individuals. Eliminate non-physically plausible individuals. Evaluate the objective values of all individuals, and determine x_{best} which has the best objective value.

Step 3: Perform mutation operation for each individual according to Equation (4.11) in order to obtain each individual's mutant counterpart.

Step 4: Perform crossover operation between each individual and its corresponding mutant counterpart according to Equation (4.14) in order to obtain each individual's trial individual.

Step 5: Evaluate the objective values of the trial individuals.

Step 6: Perform selection operation between each individual and its corresponding trial counterpart according to Equation (4.15) so as to generate the new individual for the next generation.

Step 7: Check all individuals. If a candidate parameter set is not a physically plausible solution, then an exaggerated cost function value is returned. Eliminate the "unstable" individuals.

Step 8: Determine the best individual of the current new population with the best objective value. If the objective value is better than the objective value of x_{best}, then update x_{best} and its objective value with the value and objective value of the current best individual.

Step 9: If a stopping criterion is met, then output x_{best} and its objective value; otherwise go back to Step 3.

4.4 Symbolization-based Differential Evolution Strategy

In this section, a hybrid strategy was devised, called the symbolization-based differential evolution strategy (SDES), which combines the respective merits of STSA and DE.

In research field of structural system identification, usually a comparison of the time response of the system with that of a parameterized model using a norm or some performance criterion can give us a measure of how well the model explains the system.

Procedure of SDES will be explained using a physical system with input u and output y. Let $y(t_i)$ $(i = 1, \dots, T)$ denote the value of the actual system at the ith discrete time step. Suppose that a parameterized model able to capture the behavior of the physical system is developed and this model depends on a set of n parameters, i.e., $x = (x_1, x_2, \dots, x_n)^T \in R^n$. Given a candidate parameter value x and a guess $\hat{X}_0$ of

the initial state, $\hat{y}(t_i)$ $(i = 1, \dots, T)$, the value of the parameterized model, i.e., the identified system at the ith discrete time step can be obtained. Hence, the problem of system identification boils down to finding a set of parameters that minimize the prediction error between the system output $y(t_i)$, which is the measured data, and the model output $\hat{y}(x, t_i)$, which is calculated at each time instant t_i .

Usually our interest lies in minimizing the predefined error norm of the time series outputs, e.g., the following mean square error (MSE) function,

$$f(x) = \frac{1}{T}\sum_{i=1}^{T}\|y(t_i) - \hat{y}(x, t_i)\|^2 \tag{4.16}$$

where $\|\cdot\|$ represents the Euclidean norm of vectors. Formally, the optimization problem requires one to find a set of n parameters $x^* \in R^n$, so that a certain quality criterion is satisfied, namely, that the error norm $f(\bullet)$ is minimized. The function $f(\bullet)$ is called a fitness function or objective function. Typically, an objective function that reflects the goodness of the solution is chosen. The identification problem can thus be treated as a linearly constrained multi-dimensional optimization problem, namely:

$$\begin{aligned} &\text{Minimize} \quad f(x), x = (x_1, x_2, \dots, x_n)^T \\ &\text{s.t.} \quad x \in S,\ S = \left\{x: x_{min,i} \le x_i \le x_{max,i}, \forall i = 1,2, \dots, n\right\} \end{aligned} \tag{4.17}$$

where $f(x)$ is an objective function which maps the decision variable x into the objective space $f = R^n \to R$, S is an n-dimensional feasible search space, and x_{max} and x_{min} denote the upper bounds and the lower bounds of the n parameters, respectively.

In SDES, response time histories of the system and the model should be firstly symbolized and transformed into corresponding SSH respectively using the method stated in Chapter 2. The RSSHe of the normalized state frequency vectors, Equation (2.2), is used as the objective fitness function.

Differential Evolution (DE) algorithm is then employed to solve this optimization problem. u is input signal as ground motion, y is output information as raw acceleration data, D and $\widehat{D}$ are SSHs transformed from the raw acceleration data of system and model, respectively. Stopping criterion can be reached by adjusting the model parameters x, the corresponding model parameters are identified as the system parameters (see Figure 4.1).

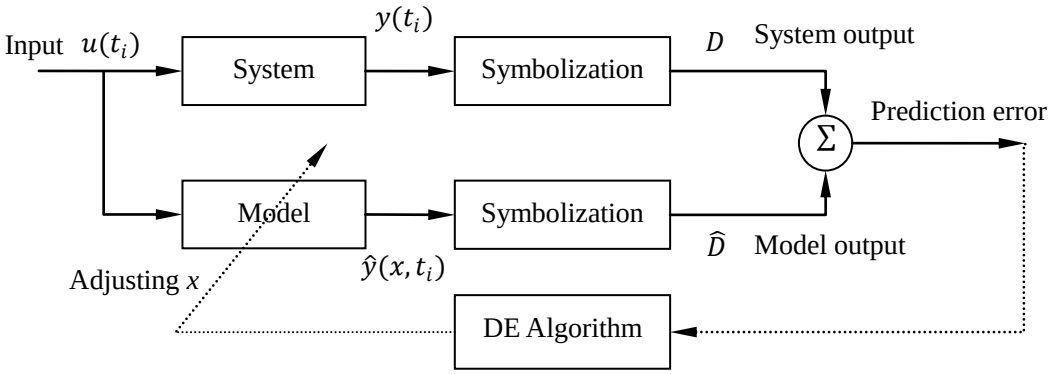

Figure 4.1. Procedure of SDES

4.5 Effects of Solution Range

As using the procedure that was discussed previously in section 2.6, the solution range can be illustrated. A numerical model representing a five-story shear frame structure is used as an example. As the existence of solution range is considered as one feature of symbolization, no noise is added to the raw acceleration data. Structural parameters

are listed in Table 4.1 under label "stiff" model type. The initial candidate solution space for each story is [1.00×10^{6}N/m, 4.00×10^{6}N/m], and noise free signal is used. Employing the procedure of searching solution range with the excited input as Gauss white noise (Gauss), and also the word length varied from 1 to 12 with "Mean" symbolization strategy. The number of candidate stiffness vector in current solution space, N_c=10,000 and the solution space reduce rate, P=1.05. The results are shown in Figure 4.2, where $\theta = \frac{\Delta B_N}{k_T} = \frac{B_N^R - B_N^L}{k_T}$ is width of the solution range with respect to the true solution.

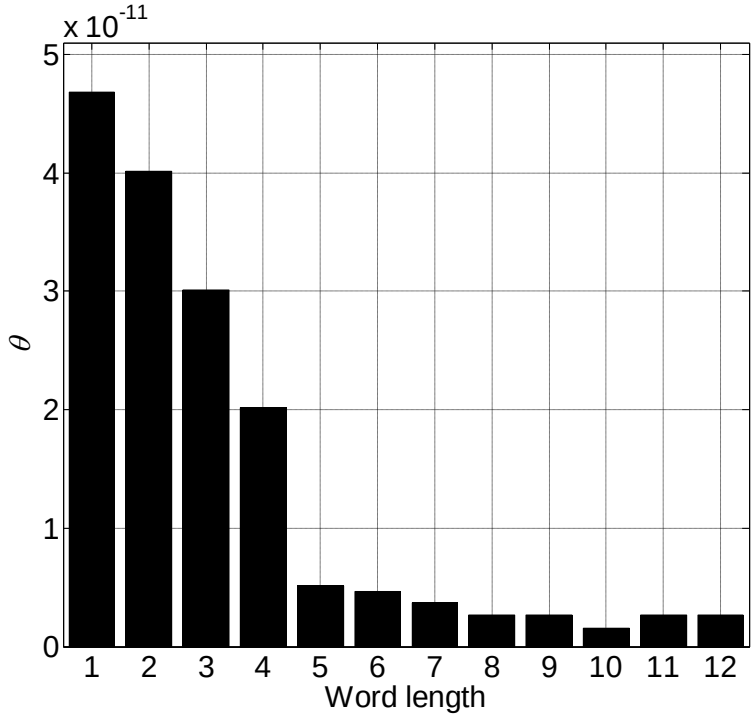

Figure 4.2. Solution range of symbolization using Gaussian white noise (Gauss)

Taking the case of using 9 to be word length as an example, θ is 2.69×10^{-12}. This solution range is small enough to be close to k_T. Considering the numerical limitation on precision, the effects of SDES on accuracy can be negligible.

4.6 Numerical Simulation

The factors that may affect the performance of SDES include the word length, structure type, partition strategy, number of sensors, and also existence of noise. The effect of these factors will be verified in this section and also the performance of SDES will be compared with other existing methods.

4.6.1 Numerical Verification

Because the goal of this research was to choose appropriate parameters for SDES and verify its performance, a shear frame structure was used for simplicity and generality. We used a five-story shear frame structure and modeled it as a multiple degree-of-freedom lumped mass system having the structural parameters and modal parameters shown in Tables 4.1 and 4.2. The schematic diagram of the structure is the same as that of Figure 3.3 .

Table 4.1. Structural parameters of different objective systems

Model type	DOF	1	2	3	4	5
Stiff	Mass (kg)	1000	1000	1000	1000	1000
	Stiffness ($\times 10^6$N/m)	2.00	2.00	2.00	2.00	2.00
Soft	Mass (kg)	1000	1000	1000	1000	1000
	Stiffness ($\times 10^5$N/m)	1.00	1.00	1.00	1.00	1.00

Table 4.2. Modal parameters of different objective systems

Model type	DOF	1	2	3	4	5
Stiff	Frequency (Hz)	2.03	5.91	9.32	11.98	13.66
Soft	Frequency (Hz)	0.45	1.32	2.08	2.68	3.05

In the following section, the five-story structure with a stiffness of 2.00×10^6 N/m on every story is called "stiff". The other structure is called "soft".

The damping matrix was assumed to be Rayleigh damping of the following form:

$$C = \alpha M + \beta K \tag{4.18}$$

where α is the mass-proportional Rayleigh damping coefficient, β is the stiffness-proportional Rayleigh damping coefficient, M is the system structural mass matrix and K is the system structural stiffness matrix.

The damping ratios of the first and the second modes ξ_1 and ξ_2 were set to be 0.03 and 0.05, respectively. α and β were obtained according to:

$$\alpha = \frac{2\omega_1\omega_2(\xi_1\omega_2-\xi_2\omega_1)}{{\omega_2}^2-{\omega_1}^2};\ \beta = \frac{2(\xi_2\omega_2-\xi_1\omega_1)}{{\omega_2}^2-{\omega_1}^2}; \tag{4.19}$$

where ω_1 and ω_2 are the circular natural frequencies of the first and the second modes.

A raw acceleration time series $\{\ddot{x}_0, \ddot{x}_1, \dots, \ddot{x}_{T-1}\}$ of length T was generated by iterating the nominal system with a nominal parameter value γ^0, which included mass, stiffness, and damping. The initial state X_0 included the initial displacement and velocity:

$$X_{t+1} = f(X_t, \gamma^0),\ Y_{t+1} = G_t + w_t = g(X_t, \gamma^0) + w_t. \tag{4.20}$$

where w_t is white noise, levels includes 0, 5%, 10% and 25%. The search domain is multi dimensional hyperrectangle $H = \{\hat{\gamma}|0.5\gamma^0 \leq \hat{\gamma} \leq 2\gamma^0\}$. The initial candidate solution was randomly created, the maximum iterations numbered 500, and the error tolerance for the solution was zero. The searching procedure employing SDES was repeated 10 times, each time randomly picking the initial candidate solution.

Input signal is Real earthquake acceleration data (El Centro 1940 NS earthquake). The signals are shown in Figure 4.3.

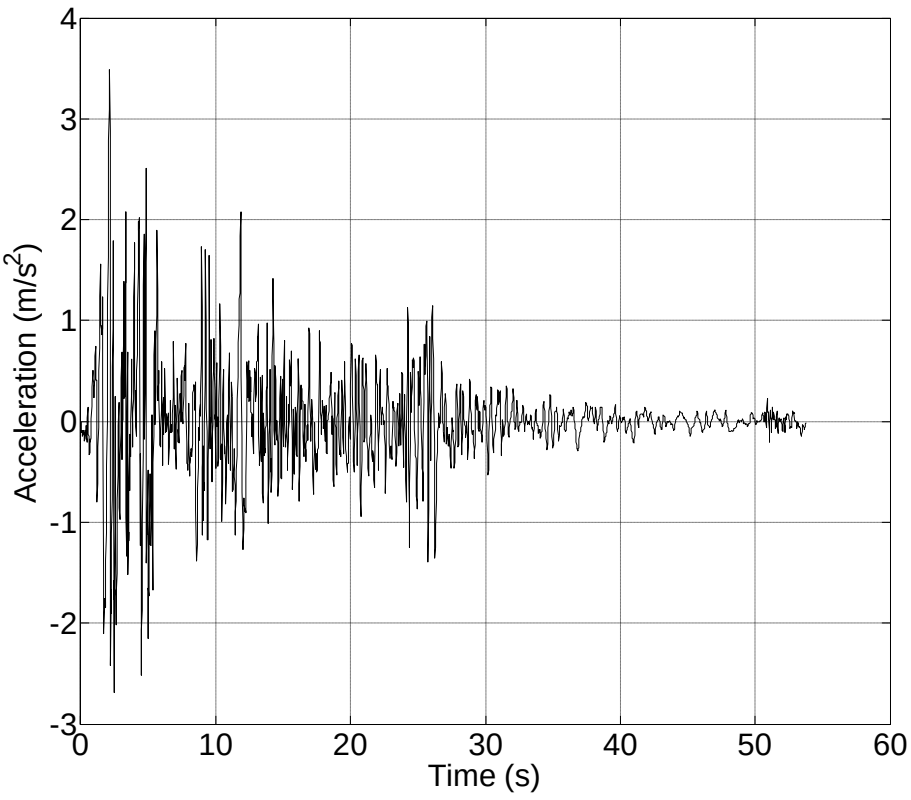

Figure 4.3. Input signal (El Centro 1940 NS earthquake)

The key parameters used in the DE algorithm of the simulation are:

$$N_P = 30;\ C_R = 0.9;\ E = 0.75;$$

where N_P is the number of agents in the population, C_R is the crossover probability constant, and E is the DE step size.

The root-mean-square error (RMSe) was used to verify the feasibility and performance of SDES. RMSe is defined as:

$$RMSe = \sqrt{\frac{\sum_{i=1}^{n}(k_{c,i}-k_{real\ ,i})^2}{\sum_{i=1}^{n} k_{real\ ,i}^2}} \tag{4.21}$$

where $k_{c,i}$ and $k_{real\ ,i}$ are the candidate stiffness and the real stiffness of the ith story, respectively.

4.6.2 Effect of Word Length

The word length should primarily capture the main dynamic characteristics of the objective system. Numerical simulations were done for the same situation but without a word length. The objective system was the 'stiff' one, and the simulation used the record of the El Centro earthquake as input, a partition strategy using zero as the partition line, and a noise level of zero. The mass distribution was assumed to be known, the stiffness of each story and damping parameters α and β were set as the objective parameters that needed to be identified. The results are listed in Table 4.3 and plotted in Figure 4.4.

Table 4.3. Performance comparison for different word lengths (T = 3000 and r = 3~12)

RMSe	Word length									
	3	4	5	6	7	8	9	10	11	12
Mean (%)	2.94	0.90	0.53	0.36	0.34	0.18	**0.18**	0.25	0.27	0.22
Max (%)	7.23	2.90	1.07	0.60	0.68	0.35	**0.37**	0.40	0.41	0.39

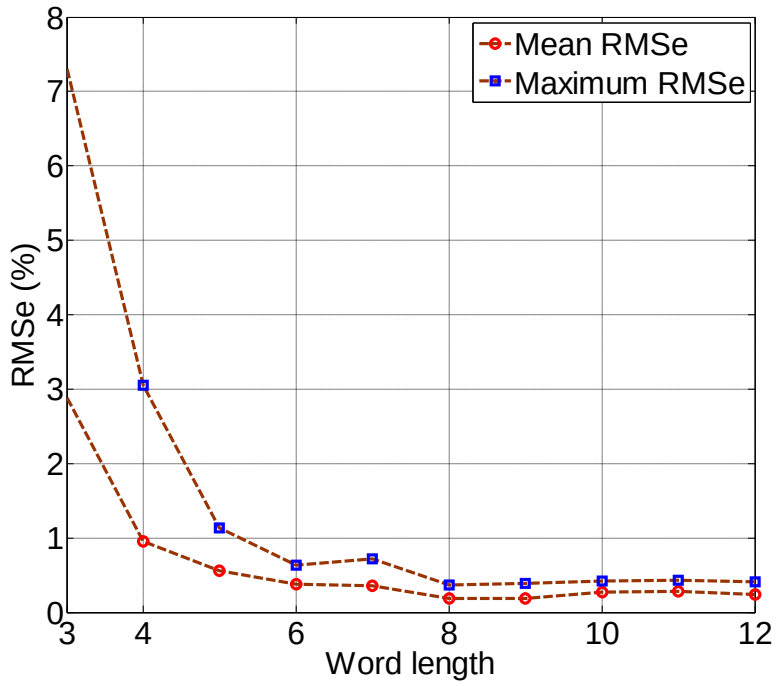

Figure 4.4. Performance comparison for different word lengths (r = 3~12)

Figure 4.4 indicates that the word length greatly affects the performance of SDES. A longer word gives better performance; the reason is that a longer word can symbolize the raw acceleration data much more accurately than a shorter one. As more dynamic information of the system is captured, the identified results become more accurate, and the maximum and the mean RMSe decrease simultaneously. The variance also decreases, which means that the estimate becomes much more stable and reliable. In

the simulation, a word length of 9 gave the best result; the mean and maximum RMSe were 0.18% and 0.37%, respectively.

4.6.3 Effect of Different Objectives

The objective systems include a ‘stiff’ and a ‘soft’ one, which have different structural parameters and modal parameters. The ‘stiff’ system has a higher frequency, and the ‘soft’ one has a lower frequency. The effect of different objective systems on the SDES should be verified. A simulation using SDES was conducted for the same settings except the structural parameters. The input was the El Centro 1940 NS earthquake. Firstly, noise free signal is used, word length is verified from 3 to 12 for ‘stiff’ and ‘soft’ objective respectively. The results of mean RMSe is shown in Figure 4.5. The ‘stiff’ objective system using the word length of 9 (see section 4.6.2) and the ‘soft’ objective system using the word length of 11 provides the best performance.

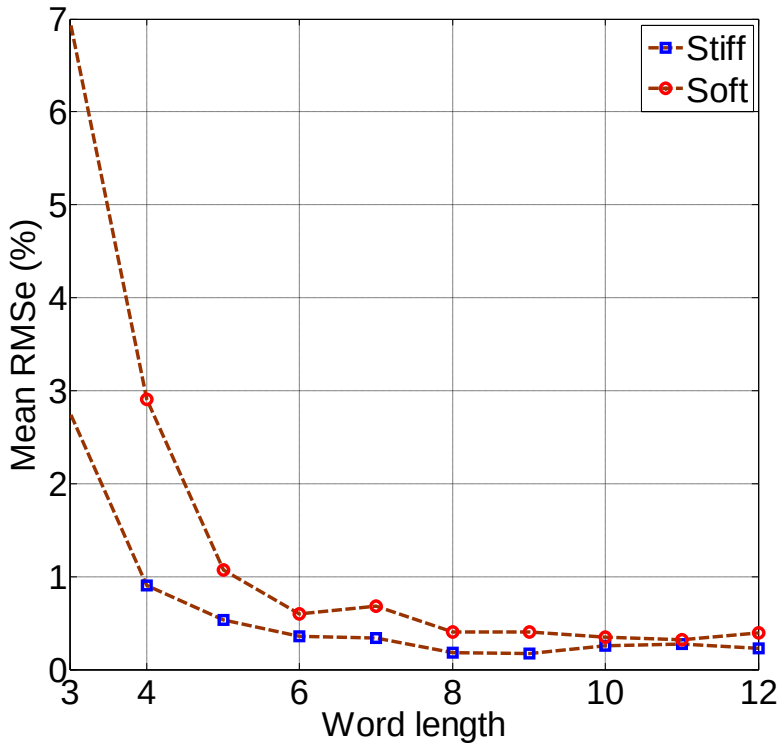

Figure 4.5. Comparison of mean RMSe between different objective systems

Then, the occurrence of noise is considered, the noise levels were 0% (i.e., no output noise), 5%, 10%, and 25%. Cases include optimal word length for different objective system, also for 'soft' system, word length 9 is chosen for comparison. Simulation results of using noise polluted signal with different noise level are in Table 4.4.

Table 4.4. Effect of different objective systems (T = 3000)

RMSe			0		5%		10%		25%	
		Word length	mean	max	mean	max	mean	max	mean	max
Objective system	Stiff	9	0.18	0.37	0.18	0.30	0.41	0.50	0.78	1.15
	Soft	9	0.64	0.92	0.35	0.49	0.78	1.01	1.59	2.00
		11	0.33	0.43	0.33	0.43	0.58	0.81	0.94	1.30

The conclusion is that the accuracy depends on the objective system. Hence, the word length should be chosen adaptively for each system.

4.6.4 Selection of Partition Strategy

In Section 2.3, we introduced different types of symbolization strategy, which are "Zero" strategy, "Mean" strategy and "1st-order difference" strategy. For a certain raw acceleration data series, different strategy will give out different SSH. The performance of employing different strategy is verified. The initial parameters were the same as above, and the full output information was used. The noise level was 0, 5%, 10% and 25%. The word length was 9. The simulation was repeated 10 times (each time randomly picking the initial candidate solution) for each case, independently. Figure 4.6 plots the maximum RMSe and mean RMSe.

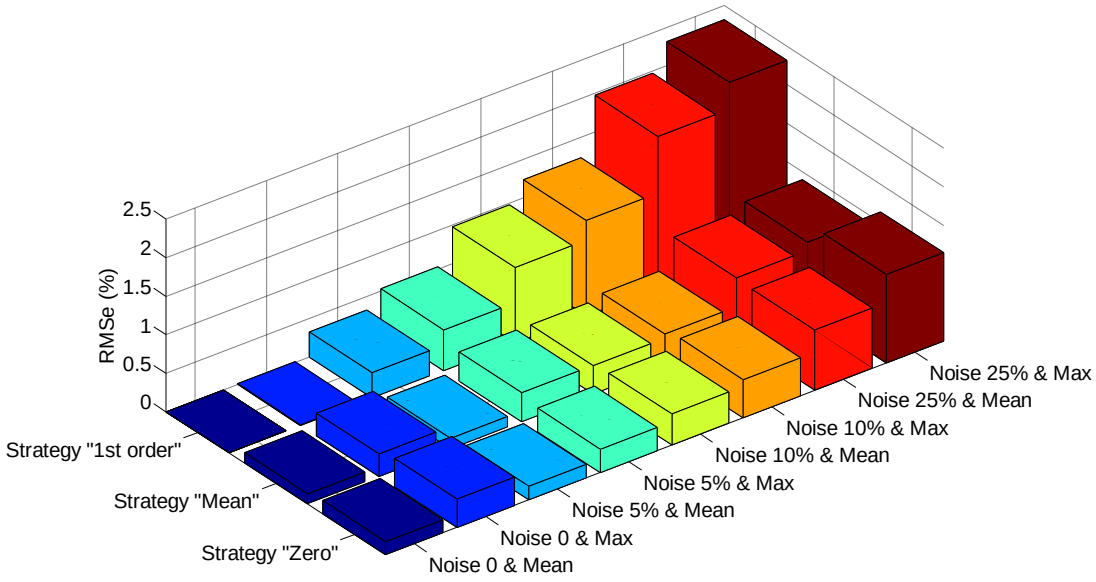

Figure 4.6. RMS errors of different partition strategies

From Figure 4.6, it is clear that the "Zero" strategy or the "Mean" strategy performs much better than the "1st-order difference" strategy. For noise-free cases, the strategy of the "1st-order difference" performs well, but it becomes worse as the noise increases.

4.6.5 Verification of Partial Output

The simulations shown above are based on the full-output information of structural acceleration data. In order to verify the performance of using only partial output information by employing the proposed methods, we analyze the "stiff" structure. Only using partial output information means only acceleration data from partial stories of the structure are used, cases include acceleration only from 1 to 5 stories and the story number in each case are randomly chosen. The simulated output data of noise-free, and with 5% noise, 10% noise, 25% noise are also in consideration. The results are shown in Figure 4.7. Symbolization strategy is "Mean" and word length of 9 is chosen.

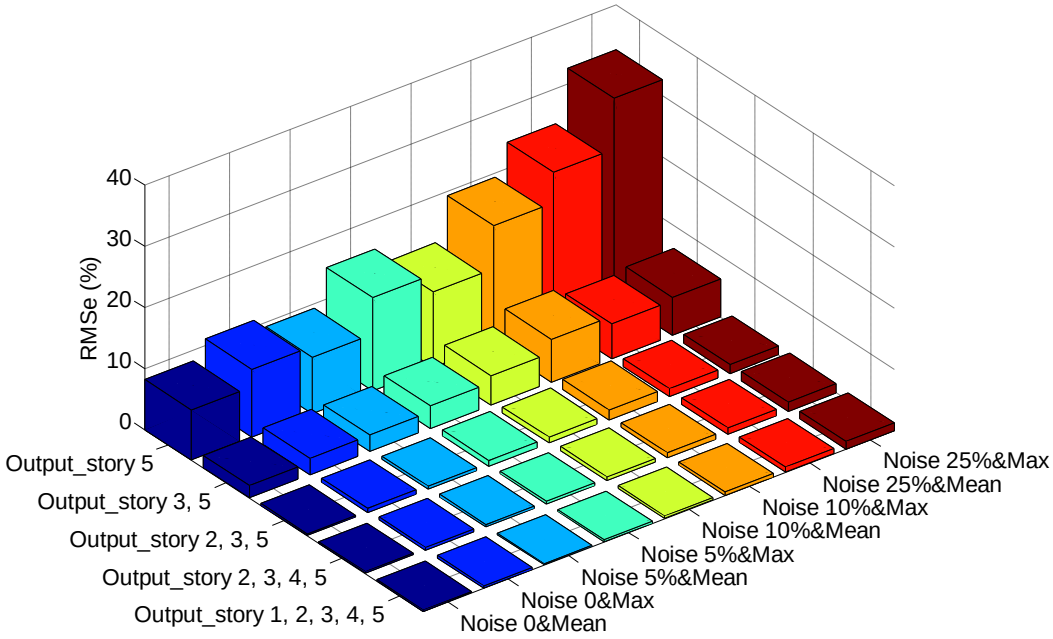

Figure 4.7. Comparison of RMSe due to partial output information

From Figure 4.7 we can see that even using partial stories' acceleration, the proposed method can obtain acceptable results except the case that only acceleration from one story is used.

4.6.6 Comparison with Other Methods

SDES was compared with differential evolution (DE) and particle swarm optimization (PSO) on raw acceleration data. The DE has been explained in Section 4.3. Particle swarm optimization (PSO) was introduced by Eberhart and Kennedy (1995). It was inspired by the social behavior of flocking birds or schooling fish. PSO shares many similarities with evolutionary computation techniques such as genetic algorithm (GA) and evolution algorithm (EA). PSO has been employed to do identification of structural parameters by Xue et al. (2009). Parameters of PSO are the same as that in (Xue et al., 2009).

The DE has been proved to be outstanding in comparison to the other algorithms (PSO and EAs). It is simple, robust, converges fast. In addition, it has few parameters to set, and the same settings can be used for many different problems (Vesterstrom and Thomsen, 2004). When faced with the system identification problem (as an optimization problem) to solve, the DE can rightfully be regarded as an excellent first choice.

In the simulations, objective function of DE and PSO with raw acceleration data is Euclidean distance of raw acceleration data series of system and candidate model, objective function of SDES is RSSHe of SSHs the transformed from raw acceleration data series of system and candidate model. For comparison, the same termination criterion is predefined for DE with raw acceleration data, PSO with raw acceleration and SDES, which is the maximum iterations numbered 500, and the error tolerance for the solution was zero.

The results are summarized in Table 4.5 and Figure 4.8.

Table 4.5. Comparison of RMSe using DE with raw acceleration, PSO with raw acceleration and SDES

Noise level	RMSe	DE with Raw acc	PSO with Raw acc	SDES
0	Mean (%)	3.94×10^{-11}	9.83×10^{-9}	0.18
	Max (%)	5.32×10^{-11}	7.96×10^{-7}	0.37
5%	Mean (%)	0.20	0.70	0.18
	Max (%)	0.21	0.95	0.30
10%	Mean (%)	0.69	1.61	0.41
	Max (%)	0.91	1.93	0.50
25%	Mean (%)	1.21	2.51	0.78
	Max (%)	1.40	2.97	1.15

For the noise-free cases, PSO and DE performed better on raw acceleration data. However, SDES provided much better estimates for data contaminated with noise. These results clearly show that SDES has excellent noise immunity.

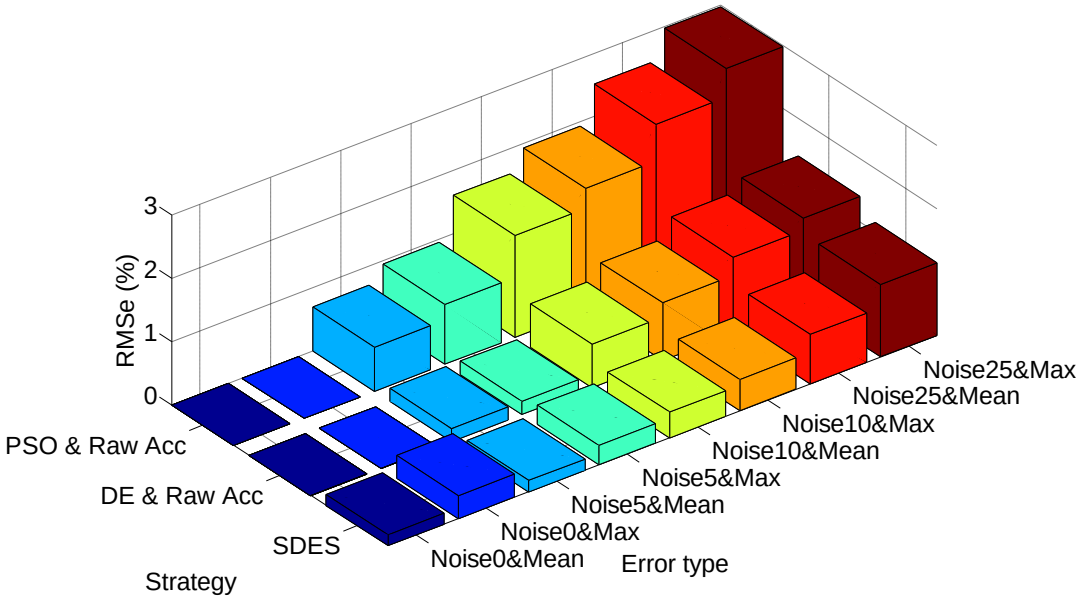

Figure 4.8. RMSe for DE and raw Acc, PSO and raw Acc, and SDES

4.7 Conclusions

The symbolization-based differential evolution strategy (SDES) is a new identification method for structural parameters that combines the merits of symbolic time series analysis and differential evolution. A symbolization of raw acceleration data enables to alleviate the harmful influence of noise. In numerical simulations and experiments, SDES exhibited very good performance when signals are contaminated by noise. The proposed SDES is a powerful tool for identifying unknown parameters of linear structural systems under noise-contaminated signals. However, comparing with DE using raw acceleration, a little more computational time is needed for the process. In addition, the method was verified only for linear structures. Thus applicability to nonlinear structural behaviors is not ensured.

CHAPTER 5
Experimental Verification and Application

5.1 Introduction

To better assess the performance of the symbolization-based intelligent algorithms for structural parameters identification that proposed above, experimental validation of the proposed approach has been conducted. Following the detailed description of the experimental setups, experimental results are provided which show the proposed approach to be very promising. Two different structural models, a small model and a large steel model, are utilized to verify the proposed approach. A five-story structure was initially healthy with all original columns intact. Two columns of one floor were then replaced by weak columns (of the same material and integrity as healthy columns, but with smaller cross-sectional area) to simulate a single-damage case. The double-damage or triple-damage case was simulated by replacing the columns of two or three different stories, respectively. Under the basement of the structure, there were some bearings so that the structure could have a ground motion. Another steel structure on a shake-table (carried out under the US–Japan cooperative structural

research project on Smart Structure Systems) was used to verify the proposed method. It was also a five-story frame structure, with a height of 5 m and a floor slab of 3 m x 2 m. The damages were introduced by removing the splices at different location, loosing the bolts and damaging the beams.

5.2 Small model

5.2.1 Experimental Setup

A series of experiments were performed to verify the performance of our proposed approach. The small model structure is depicted in Figure 5.1.

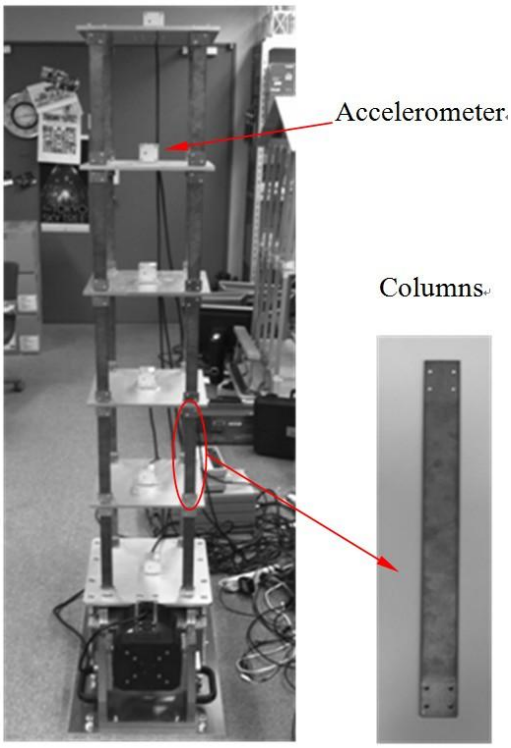

Figure 5.1. Experimental setup of small model

This experimental setup imitates a five-story shear frame buildings. The story mass is decided by the aluminum floor slab which is 2.43 kg for each floor. The story stiffness is decided by the bronze plate spring with the size of 0.0025m×0.030m×0.24 m. The Young's modulus of bronze is 1.00×10^{11} N/m^2, so the interfloor stiffness is 1.36×10^4 N/m. The structure was initially healthy with all original columns intact, and the natural frequency of the first to the fifth mode is 3.39Hz ,9.89Hz, 15.59Hz, 20.03 Hz and 22.84 Hz, respectively.

The damage was introduced by replacing columns by weak columns with the size of 0.0030m×0.0060m×0.24 m, shown in Figure 5.2. By replacing two columns in a story, the story stiffness was reduced by 33%.

Figure 5.2. Healthy (Left) and Damaged (Right) Columns

Under the basement of the structure, there were some bearings so that the structure could have a ground motion. The force input to the structure is provided with an

electrodynamic shaker as shown in Figure 5.3. One acceleration sensor was installed on the basement to measure the ground motion. The sensor installed on each floor plate was used to measure the acceleration response of each floor.

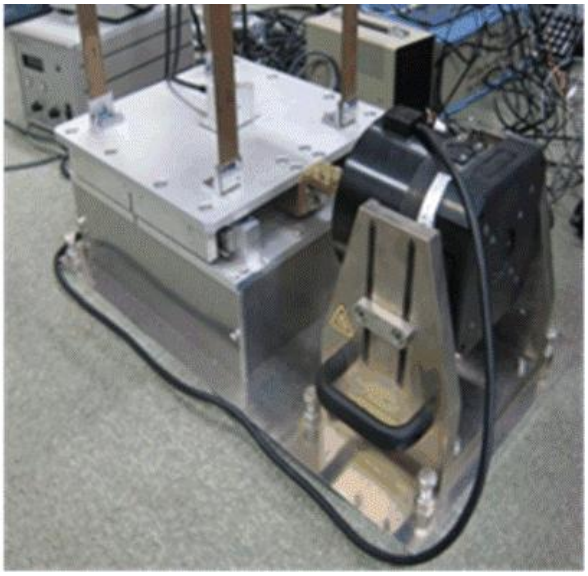

Figure 5.3. Bearings and Shaker

5.2.2 Procedure

The five-story structure was initially healthy with all original columns intact. The force input to the structure was provided by the shaker to obtain the acceleration data of the 5th story of the structure in normal state. Two acceleration sets were recorded, one of which was used as training data to generate detectors. The other set was self test data used for comparison with non-self test data.

Then, two columns of the first story were then replaced by weaker columns (of the same material and integrity as healthy columns but with a smaller cross-sectional area) to simulate the abnormal state of the structure as stiffness reduction at a single

story. The abnormal state of stiffness reduction at two stories was simulated by replacing two columns of the 1st story as well as those of the 3rd story. Finally, two columns of the 5th floor were also replaced to simulate the abnormal state case of stiffness reduction at three stories.

For each abnormal state case, the response of the experimental structure in abnormal state under another ground motion was recorded, which will be used as non-self data in the testing set.

For all cases of structure at normal or abnormal state, to localize or quantify the damage, all the acceleration data from the stories were recorded, and one set recorded from the base was used as ground acceleration data in the structural system identification employing SDES. The relative acceleration data between the five stories and the base were used as the output acceleration of the corresponding story. By using the SDES in Figure 4.1, the stiffness of each story can be identified, comparing with the original value of the healthy structure, location and degree of damage can be determined.

For only small completely vibration of the experimental setup is needed, and also considering avoiding the resonance region, a 1.1-Hz sine wave was used as the input signal in the experiments. Part of the input signal (0 to 20 s) is shown in Figure 5.4. The response of the experiential structure was recorded for 30s at a sampling frequency of 100 Hz; the total data length was 3000.

5.2.3 Damage Identification Results

The first phase, damage occurrence alarm by SNS was performed. All the parameters used were the same as those stated in the numerical simulation. Corresponding to the numerical simulation, the ANN and SVM were also employed to do the damage

detection for comparison. The results are shown in Table 5.1 and Figure 5.5.

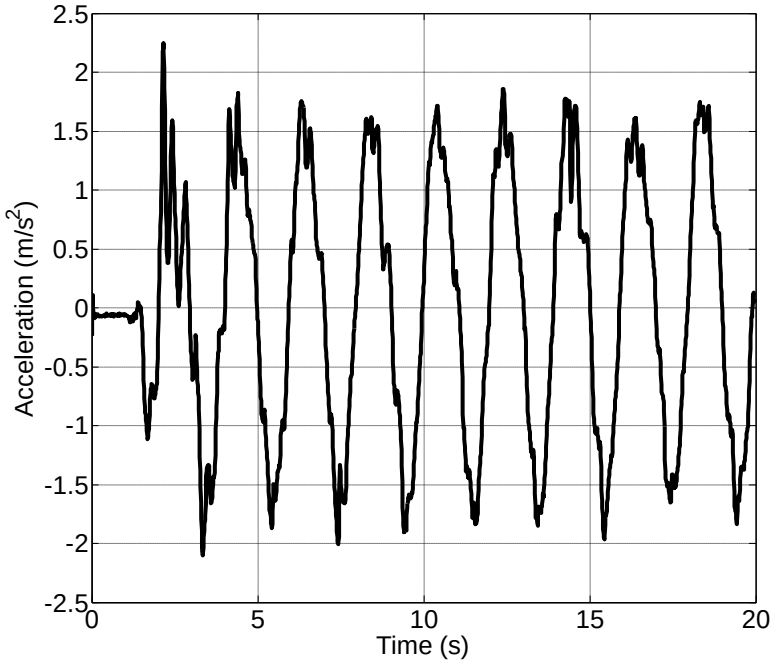

Figure 5.4. One typical acceleration signal

Table 5.1. Experimental verification of SNS, ANN, and SVM

Damage case	SNS		ANN		SVM	
	DR (%)	FAR (%)	DR (%)	FAR (%)	DR (%)	FAR (%)
One	**99.47**	**0.01**	94.60	2.49	89.71	4.25
Two	**100**	**0**	97.38	1.76	92.39	3.85
Three	**100**	**0**	96.18	2.01	91.04	4.56

The conclusion from Table 5.1 and Figure 5.5 is that no matter the number of stories, the occurrence of the abnormal states of a structure can be detected by using SNS.

Compared with the results from using the ANN and SVM, the superiority of SNS is obvious when comparing with both the DR and FAR.

The second phase was performed after knowing there was some damage in the structure. The estimated stiffness was obtained by employing SDES to minimize the error between the simulated state frequency and that of the physical structure. The identification process was repeated 10 times. The parameters of SDES were the same as those in the numerical simulation. The results are shown in Table 5.2, the unit is 10 kN/m.

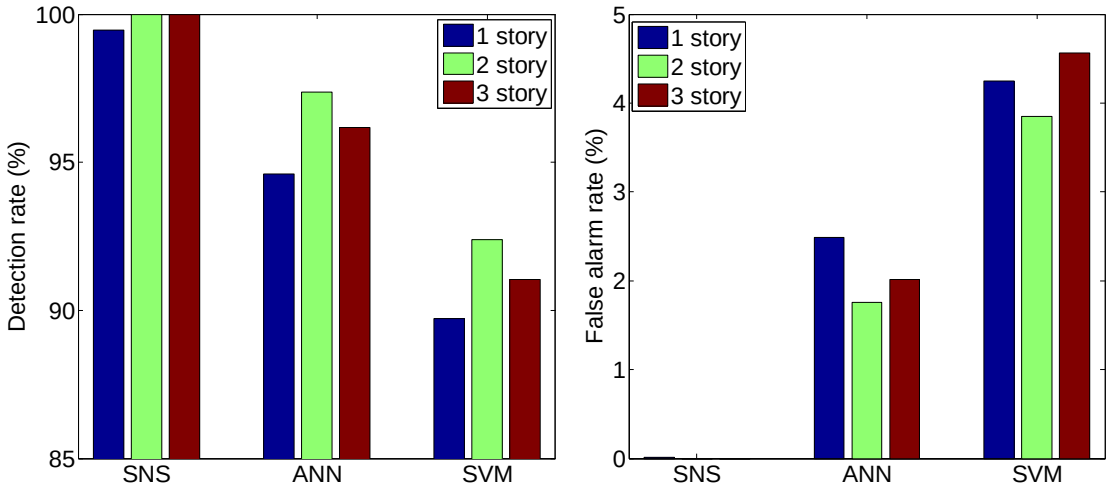

Figure 5.5. Comparison of damage detection results of SNS, ANN and SVM

The average of RMSe was 2.95%, and the largest RMSe was 3.56%. The results show that SDES can identify the structural parameters of the model quite well. For comparison, DE and PSO were performed on the raw acceleration data. Table 5.3 and Table 5.4 list the results. And the results of parameters identification by employing SDES, DE with raw acceleration and PSO with raw acceleration were compared and

shown in Figure 5.6.

The results summarized in Tables 5.2, 5.3, 5.4 and Figure 5.6 show that RMSe is much smaller with SDES than with the other methods. Also, corresponding to the section of numerical simulation, partial output cases are also verified experimentally. The cases of partial output are chosen same as that in numerical simulation for comparison, every case is calculated 10 times independently and average RMSe can be obtained. The average RMSe for each case from only one output to full output be used is 9.13%, 7.91%, 5.31%, 4.00% and 2.94% respectively. The trend is same as that of numerical simulation. The performance of SDES with partial output is acceptable.

Table 5.2. Results of experimental verification of SDES. (Unit is 10 kN/m)

	True stiffness	Process number									
		1	2	3	4	5	6	7	8	9	10
k1	1.36	1.36	1.40	1.35	1.40	1.36	1.30	1.29	1.40	1.41	1.35
k2	1.36	1.30	1.31	1.29	1.30	1.34	1.33	1.32	1.33	1.30	1.33
k3	1.36	1.36	1.37	1.40	1.35	1.31	1.39	1.30	1.32	1.36	1.28
k4	1.36	1.33	1.35	1.36	1.33	1.34	1.32	1.30	1.40	1.38	1.39
k5	1.36	1.29	1.33	1.30	1.30	1.30	1.35	1.36	1.30	1.30	1.32
RMSe (%)	0.00	3.03	2.24	3.00	3.07	2.49	2.75	3.56	3.06	3.16	3.08

Table 5.3. Results of experimental verification of DE and raw acceleration. (Unit is 10 kN/m)

	True stiffness	Process number									
		1	2	3	4	5	6	7	8	9	10
k1	1.36	1.41	1.37	1.34	1.40	1.49	1.33	1.37	1.27	1.49	1.33
k2	1.36	1.20	1.29	1.22	1.30	1.60	1.31	1.20	1.36	1.21	1.37
k3	1.36	1.35	1.53	1.46	1.35	1.30	1.25	1.50	1.55	1.32	1.52
k4	1.36	1.26	1.30	1.58	1.25	1.27	1.44	1.41	1.26	1.26	1.42
k5	1.36	1.40	1.30	1.29	1.57	1.33	1.23	1.40	1.37	1.37	1.25
RMSe (%)	0.00	6.51	6.79	9.56	8.15	9.60	6.41	7.48	7.90	7.20	6.83

Table 5.4. Results of experimental verification of PSO and raw acceleration. (Unit is 10 kN/m)

	True stiffness	Process number									
		1	2	3	4	5	6	7	8	9	10
k1	1.36	1.51	1.56	1.27	1.52	1.18	1.65	1.26	1.32	1.37	1.30
k2	1.36	1.26	1.32	1.12	1.20	1.25	1.15	1.43	1.58	1.41	1.10
k3	1.36	1.13	1.64	1.21	1.22	1.66	1.23	1.66	1.39	1.59	1.37
k4	1.36	1.44	1.26	1.37	1.33	1.37	1.25	1.46	1.25	1.64	1.24
k5	1.36	1.36	1.37	1.34	1.61	1.26	1.40	1.13	1.46	1.25	1.34
RMSe (%)	0.00	10.05	12.04	9.55	12.26	12.53	13.16	13.59	8.84	12.82	9.41

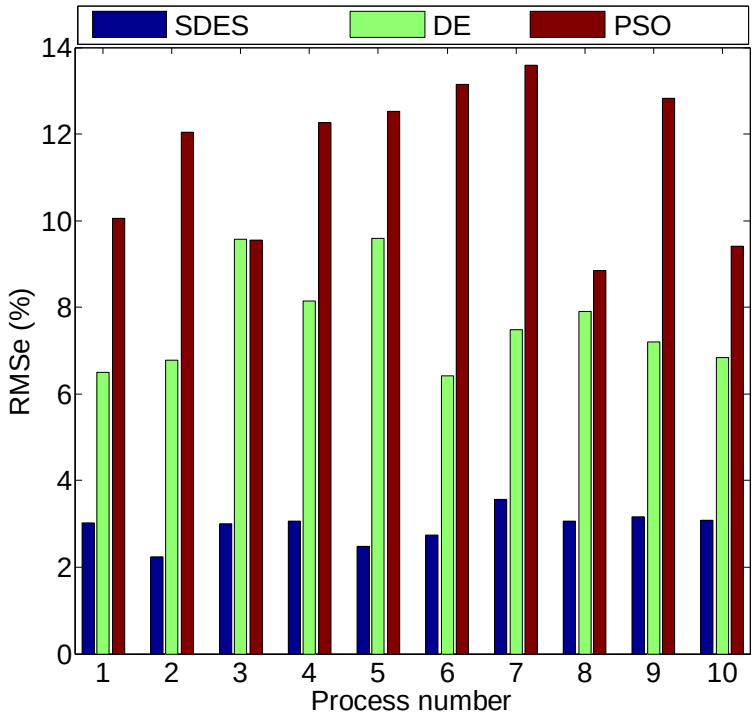

Figure 5.6. Comparison of damage identification of SDES, DE and PSO

5.3 Experiment Using Large Steel Model

5.3.1 Experimental Setup

A series of experiments (Morita et al., 2005) were performed for a different 5-story steel structure using a shake table (Figure 5.7). Data of the experiments was used to further verify the proposed method. The experiments using the steel model were carried out under the US–Japan cooperative structural research project on Smart Structure Systems (chairperson for the Japan side: Professor S. Otani).

This 5-story steel frame structure had a height of 5 m and a floor slab of 3 m×2 m. The section of a column is H148×100×6/9(SS400), a beam H148×100×6/9(SS400), a middle column H100×50×5/7(SS400). The weight of each floor is 2.57 ton. The natural frequency of the first to the fifth mode is 3.98Hz, 11.95 Hz, 19.42 Hz, 26.07

Hz, and 30.48 Hz, respectively.

The sensors are 1G accelerometer made by Kyowa Electronic Instruments Co., Ltd. Japan. The model is AS-1GB. The frequency response (at 23 ºC) is DC to 40 Hz, ±5%. The resonance frequency (App.) is 70 Hz.

The shake table is in the Building Research Institute (BRI), Ministry of Construction, Japan. The maximal bearing capacity is 20 ton. The maximal amplitude of shake is ±150 mm. The maximal acceleration is ±1 G. The maximal input force is 30 ton. The range of frequency is 0-50 Hz.

5.3.2 Procedure

First of all, the white noise force input to the structure was provided by the shake table to obtain the acceleration data of the healthy structure.

Damage was introduced by removing splice, loosening bolts and damaging beams at different locations. In every damage case, the white noise force input to the structure was provided by the shake table to obtain the acceleration data of the damaged structure.

Considering the damage would cause the stiffness reduction at the horizontal direction in Figure 5.7, the input provided by shake table was at the same direction so the acceleration at the direction of sensor number 6 in Figure 5.7 was utilized. Moreover the acceleration at the direction of sensor number 14 in Figure 5.7 was checked to be small enough to be ignored. The peak acceleration of the white noise force input is 0.1 G.

One typical acceleration response signal measured is as in Figure 5.8.

5.3.3 Damage Identification Results

The first phase, damage occurrence alarm by SNS, was performed. Damage was simulated by loosening bolts (Loosed), damaging beams (Damaged) and removing

splice (Removed) at the 1st, the 3rd and the 5th stories independently. DR and FAR of each case was calculated separately by using SNS. The detection results for this redundant experiment are shown in Table 5.5 and Figure 5.9.

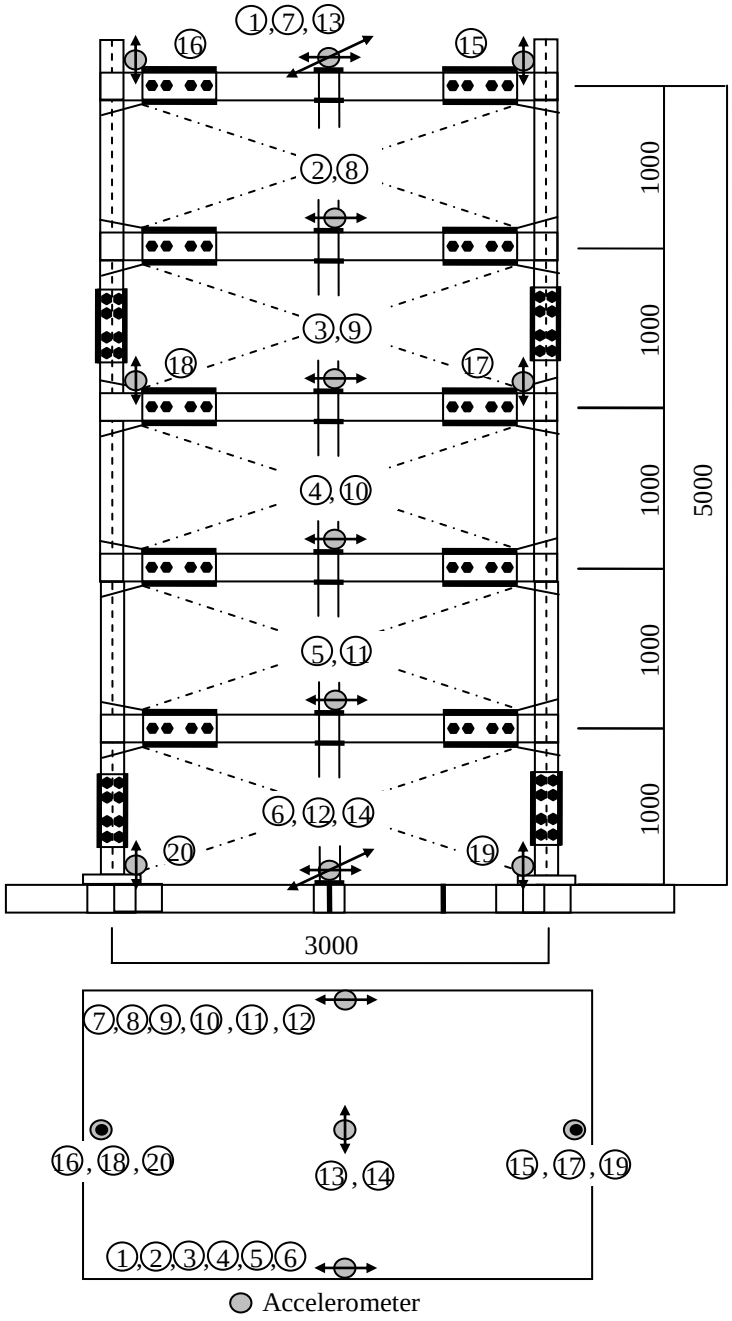

Figure 5.7. Shake-table experimental setup

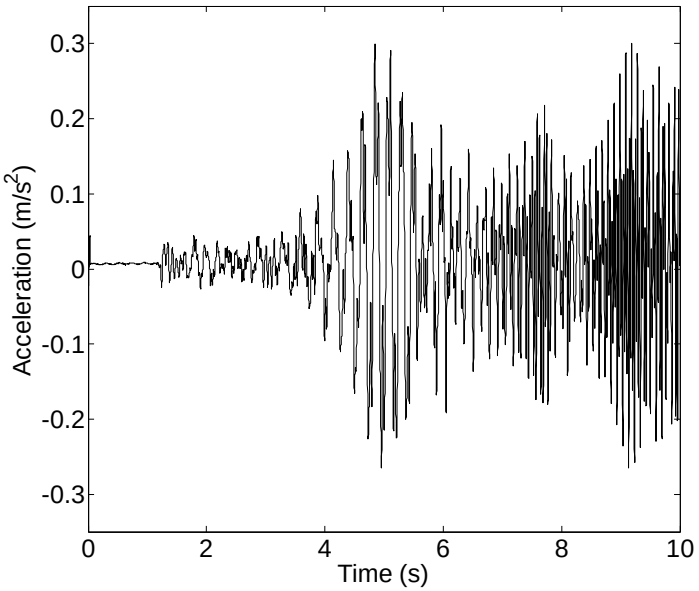

Figure 5.8. One typical acceleration response signal

Table 5.5. Experimental verification of SNS with large steel structure

Case	Loosed			Damaged			Removed		
Location	1F	3F	5F	1F	3F	5F	1F	3F	5F
DR (%)	97.64	98.03	97.91	98.91	98.78	99.31	100	99.97	99.99
FAR (%)	1.83	1.62	2.00	1.13	1.49	0.96	0.00	0.27	0.09

The analysis of the results contained in Table 5.5 and Figure 5.9 leads to observations in concordance with the first experiment: The damage detection results of detection rate and false alarm rate is acceptable no matter the location and severity of the damage. As the severity of damage increase, detection rate will increase and false alarm rate will decrease simultaneously. We may conclude that the SNS is indeed applicable to realistic problems.

The second phase was performed after knowing there was some damage in the

structure. The identification results are shown in Figure 5.10. The analysis of the results leads to the following observations: the damage location and quantity were identified for the different damage cases by the obtained stiffness reduction rate. From the figure, it can be concluded that the method is indeed applicable to realistic problems.

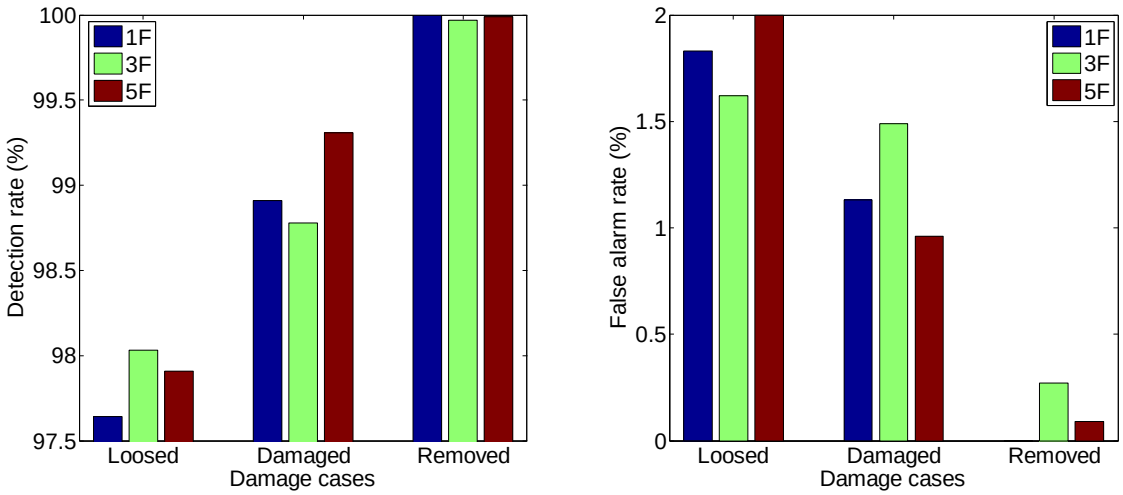

Figure 5.9. DR/FAR of experimental verification

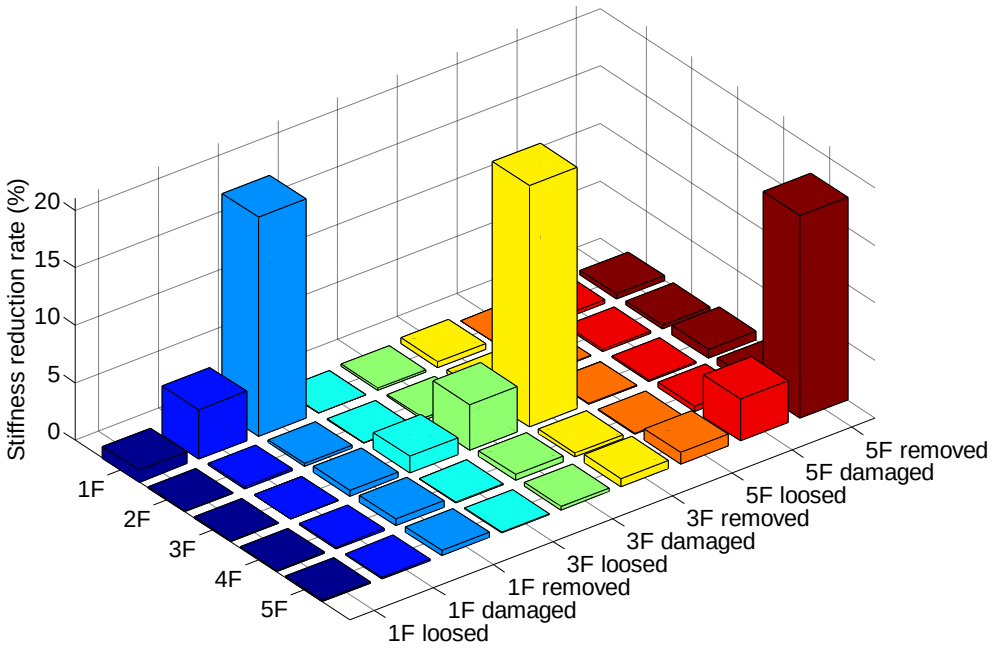

Figure 5.10. Damage localization and quantification results of shake-table experiment

5.4 Conclusions

In this chapter, the computing strategy for SHM was experimentally verified using two structural models, a small model and a large steel model. A five-story structure was initially healthy with all original columns intact. Two columns of one floor were then replaced by weak columns to simulate a single-damage case. The double-damage or triple-damage case was simulated by replacing the columns of two or three different floors, respectively. Under the basement of the structure, there were some bearings so that the structure could have a ground motion. Another steel structure on shake-table was used to verify the proposed method. It was also a five-story frame structure, with a height 5m and a floor slab of 3m x 2m. The damages were introduced by removing the splices at different location, loosing the bolts and damaging the beams. Both single and multiple damage scenarios were studied.

The experimental results have shown that the proposed approach can successfully monitor structural health only utilizing measured acceleration information for various damage scenarios under different excitation conditions. The proposed approach was shown promising for application of SHM on buildings.

At the first phase, promising results of high detection rate and low false alarm rate can be obtained even for small damage based on the verification results. During the steel structure experiment, loosing bolt only caused less than 5% stiffness reduction. In that case by employing SNS, damage alarm can be obtained. However, the localization and quantification of the damage are meant to be decided at the second phase, which was verified by the two experiments described in this chapter.

CHAPTER 6
Conclusions

Damage identification of structures using symbolic time series analysis and intelligent algorithms were addressed in this dissertation.

This research presented a new methodology for damage identification of structures using symbolic time series analysis and intelligent algorithm. Two steps were included in the damage identification process. The damage occurrence was detected in the first step using symbolization-based negative selection algorithm, while the corresponding damage location and degree were estimated in the second step using symbolization-based differential evolution strategy. A series of numerical simulations were conducted to verify the performance of our proposed approach. The measured structural vibration responses data always contain noise. The output inevitably has some errors when the data with noise was input into the intelligent algorithm. The approach was thus enhanced to have stability against such noise by employing symbolic time series analysis. The results of numerical simulations showed that by the approach the structural damage could be identified and identification accuracy could be improved by data symbolization. An appropriate range of solution was proposed corresponding to parameters in symbolic time series analysis. In order to implement

the theory in practical applications, a series of vibration experiments for five-story shear frame structure were conducted to verify the performance of the approach. The results show that for shear buildings, damage occurrence, location and degree can be identified by using our proposed methodology.

To implement the concept, a two-phase approach is proposed.

In the first phase, a symbolization-based negative selection (SNS) algorithm that combines the advantages of symbolic time series analysis (STSA) and negative selection (NS) was proposed for detecting the abnormal states of a building structure. In SNS, no prior knowledge of the structure's abnormal state is needed. Only the response of the structure in a current normal state is used as input data. In addition, this approach works fine even with one sensor, so it is highly practical and flexible. In real applications, the frequency components of input should cover all modes to be excited. Thus, the spectrum of the inputs should be wide band. Small earthquake ground motions normally include all frequency components and could be considered as input of the structure in training or detecting phase of SNS.

In the second phase, after knowing the damage occurrence, we need to determine the damage location and quantity. The method for this stage was named as “Symbolization-based Differential Evolution Strategy” (SDES). Differential evolution strategy employed here was intended to minimize the distance between SSHs that are transformed from raw acceleration data of a real structure and candidate models. Accuracy of the method was theoretically studied and explained including the effects of parameters. SDES was numerically compared with Particle Swarm Optimization (PSO) and DE with raw acceleration data. These simulations revealed that SDES provided better estimates of structural parameters when the data was contaminated by noise.

Moreover, in order to prove that the method is indeed applicable to realistic problems,

the computing strategy for SHM was experimentally verified. Two different structural models, small model and large steel model, were utilized to verify the proposed approach. Experiments using the small model were conducted at our Laboratory, damage cases were considered for different locations and degrees of damage. Data of the experiments using the steel model (carried out under the US–Japan cooperative structural research project on Smart Structure Systems) was used to further verify the proposed methodology.

Finally, the conclusion was given. The damage identification using symbolic time series analysis and intelligent algorithms was proposed, and it can detect, localize and quantify the damage accurately. The symbolization of data alleviated the effects of harmful noise, employment of the intelligent algorithms make the whole procedure adaptively and efficiently. Comparisons with existing methods showed that our proposed methodology was indeed a powerful tool for damage identification of building structures.

References

Auweraer, V., & Peeters, B. (2003). Sensors and systems for structural health monitoring. *Journal of Structural Control , 10(2)*, 117-125.

Bakhary, N., Hao, H., & Deeks, A. (2007). Damage detection using artificial neural network with consideration of uncertainties. *Engineering Structures , 29*, 2806–2815.

Bernal, D., & Hernandez, E. (2006). A data-driven methodology for assessing impact of earthquakes on the health of building structural systems. *Structural Design of Tall and Special Buildings , 15*, 21-34.

Cawley, P., & Adams, R. (1979). The location of defects in structures from measurements of natural frequencies. *The Journal of Strain Analysis for Engineering Design , 14(2)*, 49-57.

Cempel, C. (1980). Diagnostically oriented measures of vibroacoustical processes. *Journal of Sound and Vibration , 73(4)*, 547-561.

Chance, J., & Tomlinson, G. (1994). A simplified approach to the numerical and experimental modelling of the dynamics of a cracked beam. *Proceedings of the 12th International Modal Analysis Conference. ,* 778-785.

Chen, J., Chen, W., & Liang, F. (2008). T-detector maturation algorithm with overlap rate. *WSEAS Transactions on Computers, 8(7)*, pp. 1300-1308.

Cho, S., Asfour, S., Onar, A., & Kaundinya, N. (2005). Tool breakage detection using supportvectormachine learning in a milling process. *International Journal of Machine Tools and Manufacture , 45(3)*, 241–249.

Farrar, C., & Worden, K. (2007). An introduction to structural health monitoring. *Philosophical Transactions of the Royal Society A: Mathematical, Physical and Engineering Sciences , 365(1851)*, 303-315.

Forrest, S., & Perelson, A. (1994). Self-Nonself discrimination in a computer. *In Procceding of IEEE Symposium on Research in Security and Privacy*, (pp. 202-212). Oakland, CA.

Franco, G., Betti, R., & Lus, H. (2004). Identification of structural systems using an evolutionary strategy. *J Eng Mech , 130(10)*, 1125–39.

Friswell, M., Penny, J., & Wilson, D. (1994). Using vibration data and statistical measures to locate damage in structures. *Modal Analysis: The International Journal of Analytical and Experimental Modal Analysis , 9(4)*, 239-254.

Guo, H., & Li, Z. (2011). Structural damage detection based on strain energy and evidence theory. *Applied Mechanics and Materials , 48-49*, 1122-1125.

Gupta, S., & Ray, A. (2007). Pattern identification using lattice spin systems: A thermodynamic formalism. *Applied Physics Letters , 91(19)*, 194105.

Gupta, S., Ray, A., & Keller, E. (2007). Symbolic time series analysis of ultrasonic data for early detection of fatigue damage. *Signal Processing , 21(2)*, 866–884.

Gupta, S., Ray, A., & Mukhopadhyay, A. (2006). Anomaly detection in thermal pulse combustors using symbolic time series analysis. *Proc. IMechE Vol. 220 Part I: Journal of Systems and Control Engineering , 220(5)*, 339-351.

Gupta, S., Ray, A., Sarkar, S., & Yasar, M. (2011). Fault detection and isolation in

aircraft gas turbine engines: Part I - underlying concept. *Journal of Engineering for Gas Turbines and Power , 126(1)*, 55-61.

Hayton, P., & Utete, S. (2007). Static and dynamic novelty detection methods for jet engine health monitoring. *Philosophical Transactions of the Royal Society A: Mathematical, Physical and Engineering Sciences , 365(1851)*, 493-514.

Hearn, G., & Testa, R. (1991). Modal analysis for damage detection in structures. *Journal of Structural Engineering , 117(10)*, 3042-3063.

Ji, Z., & Dasgupta, D. (2006). Applicability issues of the real-valued negative selection algorithms. *GECCO*, (pp. 111-118). Seattle, Washington, USA.

Ji, Z., & Dasgupta, D. (2004). Real-valued negative selection algorithm with variable-sized detectors. *Genetic and Evolutionary Computation Conference (GECCO)* , 314-328.

Kennedy, J., & Eberhart, R. (1995). Particle swarm optimization. *Proceedings., IEEE International conference on neural networks* , 1942-1948.

Kessler, S. S., Spearing, S. M., Atalla, J. M., Cesnik, E. C., & Soutis, C. (2002). Damage detection in composite materials using frequency response methods. *Composites Part B: Engineering , 33(1)*, 87-95.

Kim, J., Ryu, Y., Cho, H., & Stubbs, N. (2003). Damage identification in beam-type structures: frequency-based method vs mode-shape-based method. *Engineering Structures , 25(1)*, 57-67.

Koziel, S., & Michalewicz, Z. (1999). Evolutionary algorithms, homomorphous mappings and constrained parameter optimization. *Evol Comput , 7(1)*, 19–44.

Lera, G., & Pinzolas, M. (2002). Neighborhood based Levenberg–Marquardt algorithm for neural network training. *IEEE transcations on neural networks , 13(5)*,

1200-1203.

Li, R., & Mita, A. (2011). Structural damage identification using adaptive immune clonal selection algorithm and acceleration data. *SPIE Smart Structures/NDE 2011 , 7981*, 191-200.

Lieven, N., & Ewins, D. (1988). Spatial correlation of mode shapes, the coordinate modal assurance criterion (COMAC). *Proceedings of the 6th International Modal Analysis Conference, Bethel* , 690-695.

Ljung, L. (1999). *System identification : theory for the user.* Prentice Hall PTR: Upper Saddle River, NJ.

Lynch, J., Wang, Y., Lu, K., Hou, T., & Loh, C. (2006). Post-seismic damage assessment of steel structures instrumented with self-interrogating wireless sensors. *Proc. of the 8th National Conference on Earthquake Engineering* , San Francisco,CA.

Mita, A. (2003). *Structural Dynamics for Health Monitoring (First Edition).* Japan: SANKEISHA Co., Ltd.: Nagoya.

Mita, A., & Hagiwara, H. (2003). Damage diagnosis of a building structure using support vector machine and modal frequency patterns. *Proceedings of the Smart Structures and Materials 2003: Smart Systems and NDE for Civil Infrastructures , 5057*, 118–125.

Morita, K., Teshigawara, M., & Hamamoto, T. (2005). Detection and estimation of damage to steel frames through shaking table tests. *Structural Control and Health Monitoring , 12*, 357–380.

Pandey, A., & Biswas, M. (1991). Damage detection from changes in curvature mode shapes. *Journal of Sound and Vibration , 145(2)*, 321-332.

Peeters, B., Maeck, J., & Guido, R. D. (2001). Vibration-based damage detection in

civil engineering: excitation sources and temperature effects. *Smart Materials and Structures , 10*, 518-527.

Price, K. (1999). An introduction to differential evolution. *In: Corne D, Dorigo M,Glover F, editors. New ideas in optimization*, (pp. 79–108). London: McGraw-Hill.

Price, K., & Storn, R. (1997). Differential evolution: numerical optimization made easy. *Dr.Dobb's J , 78*, pp. 18–24.

Qian, Y., & Mita, A. (2008). Acceleration-based damage indicators for building structures using neural network emulators. *Journal of Structural Control and Health Monitoring , 15(6)*, 901-920.

Qiao, P., & Lu, K. (2007). Curvature mode shape-based damage detection in composite laminated plates. *Composite Structures , 80(3)*, 409-428.

Rajagopalan, V., & Ray, A. (2006). Symbolic time series analysis via wavelet-based partitioning. *Signal Processing , 86(11)*, 3309–3320.

Rajagopalan, V., Chakraborty, S., & Ray, A. (2008). Estimation of slowly varying parameters in nonlinear systems via symbolic dynamic filtering. *Signal Processing , 88(2)*, 339–348.

Rajagopalan, V., Ray, A., Samsi, R., & Mayer, J. (2007). Pattern identification in dynamical systems via symbolic time series analysis. *Pattern Recognition , 40(11)*, 2897–2907.

Rao, C., Ray, A., Sarkar, S., & Yasar, M. (2009). Review and comparative evaluation of symbolic dynamic filtering for detection of anomaly patterns. *Signal, Image and Video Processing , 3(2)*, 101-114.

Ray, A. (2004). Symbolic dynamic analysis of complex systems for anomaly detection. *Signal Processing , 84(7)*, 1115–1130.

Rytter, A. (1993). *Vibration based inspection of civil engineering structures.* Denmark, Aalborg University. Ph.D: Department of Building Technology and Structural Engineering.

Rytter, A., & Kirkegaard, P. (1997). Vibration based inspection using neural networks. *Structural Damage Assessment Using Advanced Signal Processing Procedures* , 97-108.

Salawu, O., & Williams, C. (1995). Bridge assessment using forced-vibration testing. *Journal of Structural Engineering , 121*, 161-173.

Sarkar, S., Jin, X., & Ray, A. (2011). Data-driven fault detection in aircraft engines with noisy sensor measurements. *Journal of Engineering for Gas Turbines and Power-Transactions of the ASME , 133(8)*, 081602-081611.

Sarkar, S., Rao, C., & Ray, A. (2009). Statistical estimation of multiple faults in aircraft gas turbine engines. *Proceedings of the I Mech E Part G:Journal of Aerospace Engineering , 223(4)*, 415-424.

Sarkar, S., Yasar, M., Gupta, S., Ray, A., & Mukherjee, K. (2008). Fault detection and isolation in aircraft gas turbine engines: Part II - validation on a simulation test bed. *Proceedings of the I Mech E Part G: Journal of Aerospace Engineering , 222(3)*, 319-330.

Sohn, B., Czarnecki, J., & Farrar, C. (2000). Structural health monitoring using statistical process control. *Journal of Structural Engineering* , 1356-1363.

Sohn, H. (2007). Effects of environmental and operational variability on structural health monitoring. *Philosophical Transactions of the Royal Society A: Mathematical, Physical and Engineering Sciences , 365(1851)*, 539-560.

Sohn, H., & Farrar, C. (2001). Damage diagnosis using time-series analysis of vibrating signals. *Journal of Smart Materials and Structures , 10(3)*, 446-451.

Sohn, H., & Laboratory. (2004). *A Review of Structural Health Monitoring Literature: 1996-2001*. Los Alamos National Laboratory.

Storn, R., & Price, K. (1997). Differential evolution-a simple and efficient heuristic for global optimization over continuous spaces. *Journal of global optimization , 11*, 341–359.

Storn, R., & Price, K. (1996). Minimizing the real functions of the ICEC'96 contest by. *Proceedings of the IEEE international conference on* , 604-610.

Tang, H., Xue, S., & Fan, C. (2008). Differential evolution strategy for structural system identification. *Computers and Structures , 86,* 2004–2012.

Tang, H., Xue, S., Chen, R., & Sato, T. (2006). Online weighted LS-SVM for hysteretic structural system identification. *Engineering Structures , 28(12),* pp. 1728–1735.

Vesterstrom, J., & Thomsen, R. (2004). A comparative study of differential evolution, particle swarm optimization, and evolutionary algorithms on numerical benchmark problems. *Evolutionary Computation, 2004. CEC2004. Congress on , 2*, 1980-1987.

Vestroni, F., & Capecchi, D. (2000). Damage detection in beam structures based on frequency measurements. *Journal of Engineering Mechanics* , 126:761.

Wan, C., & Mita, A. (2009). Pipeline monitoring using acoustic principal component analysis recognition with the Mel scale. *Smart Materials and Structures , 18*, 055004.

Wang, J., & Ko, J. (2000). Modal sensitivity analysis of Tsing Ma Bridge for structural damage detection. *Proceedings of SPIE, Newport Beach, CA, USA.*

West, W. (1986). Illustration of the use of modal assurance criterion to detect structural changes in an orbiter test specimen. *Proceedings of the Air Force Conference on Aircraft Structural Integrity, Los Angles.*

Williams, E., & Messina, A. (1999). Applications of the multiple damage location assurance criterion. *Key Engineering Materials , 167*, 256-264.

Wolff, T., & Richardson, M. (1989). Fault detection in structures from changes in their modal parameters. *Proceedings of the 7th International Modal Analysis Conference* .

Xing, Z., & Mita, A. (2011). A substructure approach to local damage detection of shear structure. *Journal of Structural Control and Health Monitoring , 18(3)*, DOI: 10.1002/stc.439.

Xue, S., Tang, H., & Xie, Q. (2009). Structural damage detection using auxiliary particle filtering method. *Structural Health Monitoring , 8(2)*, 101-112.

Xue, S., Tang, H., & Zhou, J. (2009). Identification of structural systems using particle swarm optimization. *Journal of Asian Architecture and Building Engineering , 8(2)*, 517-524.

Yang, J., & Lin, S. (2004). On-line identification of non-linear hysteretic structures using an adaptive tracking technique. *International Journal of Non-Linear Mechanics , 39(9)*, pp. 1481-1491.

Yang, J., Lin, S., Huang, H., & Zhou, L. (2006). An adaptive extended Kalman filter for structural damage identification. *Journal of Structural Control and Health Monitoring , 13*, pp. 849–867.

Yao, J., & Natke, H. (1994). Damage detection and reliability evaluation of existing structures. *Structural Safety , 15(1-2)*, 3-16.

Zheng, H., & Mita, A. (2008). Damage indicator defined as distance between ARMA models for structural health monitoring. *Journal of Structural Control and Health Monitoring , 15(7)*, 992-1005.

Zheng, H., & Mita, A. (2007). Two-stage damage diagnosis based on the distance

between ARMA models and Pre-whitening filters. *Smart Materials and Structures , 16(2)*, 1829-1836.

Author’s biography

Rongshuai Li was born in Rizhao, China in 1983. In 2006, Rongshuai Li received the B.S. degree from Nanjing University of Technology, Nanjing, China and his research was about building design and project management, then he went to the Tongji University, Shanghai, China, for the study on wind engineering and disaster reduction. In 2009, he obtained the M.S. degree from Tongji University with the thesis “Wind effect analysis of high-speed railway catenary system”. From 2009, he studies in Mita Lab, Keio University, Japan. His research is about identification of structural parameters using symbolic time series analysis and intelligent algorithms.

List of publications

Journal Papers:

1. Rongshuai Li, Akira Mita and Jin Zhou, “Symbolization-Based Differential Evolution Strategy for Identification of Structural Parameters,” *Journal of Structural Control and Health Monitoring*, DOI: 10.1002/stc.1530, published online: 4 Nov 2012
2. Rongshuai Li, Akira Mita and Jin Zhou, “Feasibility Study of Parameter Identification Method based on Symbolic Time Series Analysis and Adaptive Immune Clonal Selection Algorithm,” *Open Journal of Civil Engineering*; DOI:10.4236/ojce.2012.24026, 2012, 2, 198-205
3. Rongshuai Li, Akira Mita and Jin Zhou, “A Hybrid Methodology for Structural Health Monitoring based on Immune Algorithms and Symbolic Time Series Analysis,” *Journal of Intelligent Learning Systems and Applications* (accepted for publication)
4. Rongshuai Li, Akira Mita and Jin Zhou, “Abnormal State Detection of Building Structures Based on Symbolic Time Series Analysis and Negative Selection,” *Journal of Structural Control and Health Monitoring* (accepted for publication)

International Conference Papers:

1. Rongshuai Li and Akira Mita, " Structural damage identification using adaptive immune clonal selection algorithm and acceleration data," *Proc. SPIE* 7981, Sensors and Smart Structures Technologies for Civil, Mechanical, and Aerospace Systems 2011, 79815A; doi:10.1117/12.879782
2. Rongshuai Li and Akira Mita, " Hybrid Immune Algorithm for Structural Health Monitoring Using Acceleration Data," 8th International Workshop on Structural Health Monitoring; Stanford University ; Stanford University ; P.1095-1102 ; 2011/09/15
3. Jin Zhou, Akira Mita, Li Rongshuai, " Multi-objective optimization strategies for damage detection using cloud model theory," Proc. of SPIE Vol. 8348 83482R-1 ; 2012/03/13